CANCER

BRAF$^{\Delta\beta3\text{-}\alpha C}$ in-frame deletion mutants differ in their dimerization propensity, HSP90 dependence, and druggability

Manuel Lauinger[1,2], Daniel Christen[1,2,3], Rhena F. U. Klar[1,2,3,4,5,6], Carole Roubaty[7], Christoph E. Heilig[8,9], Michael Stumpe[7], Jennifer J. Knox[10,11], Nikolina Radulovich[11], Laura Tamblyn[11], Irene Y. Xie[11], Peter Horak[8,9], Andrea Forschner[12,13], Michael Bitzer[13,14,15], Uwe A. Wittel[16], Melanie Boerries[3,6,17], Claudia R. Ball[18,19,20,21,22,23,24], Christoph Heining[18,19,20,21,22,23], Hanno Glimm[18,19,20,21,22,23,25], Martina Fröhlich[26], Daniel Hübschmann[9,26,27], Steven Gallinger[10,11], Ralph Fritsch[5,28], Stefan Fröhling[8,9], Grainne M. O'Kane[10,11], Jörn Dengjel[7], Tilman Brummer[1,3,4,17,29]*

Copyright © 2023 The Authors, some rights reserved; exclusive licensee American Association for the Advancement of Science. No claim to original U.S. Government Works. Distributed under a Creative Commons Attribution License 4.0 (CC BY).

In-frame *BRAF* exon 12 deletions are increasingly identified in various tumor types. The resultant BRAF$^{\Delta\beta3\text{-}\alpha C}$ oncoproteins usually lack five amino acids in the β3-αC helix linker and sometimes contain de novo insertions. The dimerization status of BRAF$^{\Delta\beta3\text{-}\alpha C}$ oncoproteins, their precise pathomechanism, and their direct druggability by RAF inhibitors (RAFi) has been under debate. Here, we functionally characterize BRAF$^{\Delta LNVTAP>F}$ and two novel mutants, BRAF^{delinsFS} and BRAF$^{\Delta LNVT>F}$, and compare them with other BRAF$^{\Delta\beta3\text{-}\alpha C}$ oncoproteins. We show that BRAF$^{\Delta\beta3\text{-}\alpha C}$ oncoproteins not only form stable homodimers and large multiprotein complexes but also require dimerization. Nevertheless, details matter as aromatic amino acids at the deletion junction of some BRAF$^{\Delta\beta3\text{-}\alpha C}$ oncoproteins, e.g., BRAF$^{\Delta LNVTAP>F}$, increase their stability and dimerization propensity while conferring resistance to monomer-favoring RAFi such as dabrafenib or HSP 90/CDC37 inhibition. In contrast, dimer-favoring inhibitors such as naporafenib inhibit all BRAF$^{\Delta\beta3\text{-}\alpha C}$ mutants in cell lines and patient-derived organoids, suggesting that tumors driven by such oncoproteins are vulnerable to these compounds.

INTRODUCTION

The serine/threonine kinases of the RAF family comprise the ARAF, BRAF, and RAF1 isoforms and represent critical signaling elements in the RAS/RAF/mitogen-activated protein kinase (MAPK) kinase (MEK)/extracellular signal–regulated kinase (ERK) pathway. RAFs, in particular the frequently mutated BRAF isoform, emerged as major drug targets in oncology (*1*). RAF becomes activated by RAS-mediated membrane recruitment, which in turn promotes the transition from a closed autoinhibited to an open conformation in which the exposed kinase domains are activated by dimerization-induced allosteric transactivation (*2*, *3*). The mechanisms leading to physiological and oncogenic RAF activation are best understood from a structural perspective (*4*–*6*). RAFs share three conserved regions (CRs): CR1 and CR2 mediate RAS and 14-3-3 binding, respectively, thereby controlling membrane recruitment and the degree of autoinhibition (*4*, *7*). Among other features, the CR3 encompasses the kinase domain, which displays the typical organization of an N- and C-lobe. The kinase domain contains a dimer interface (DIF), which comprises several noncontiguous residues in both lobes (*8*). Of these, R509, which is located in the conserved R^{506}KTR^{509}HV motif at the C-terminal end of the αC helix, not only plays a key role in the formation and stabilization of RAF dimers (Fig. 1A) but also is essential for the allosteric transactivation of a still inactive receiver protomer by an already activated RAF protein (*9*–*12*). The binding of 14-3-3 proteins to the C-terminal end of CR3 also contributes to dimerization (*13*).

RAS recruits BRAF to the membrane and assists in its full activation by relieving the kinase domain from 14-3-3–mediated autoinhibition (*14*). The exposed kinase domain engages in homo- or heterodimerization with other RAF protomers, which in turn induces their conformational changes (*3*, *12*, *15*) that are probably accompanied by phosphorylation of the D^{594}FGLAT^{599}-V^{600}KS^{602} motif within the activation segment (AS) (*16*). While AS phosphorylation has not been observed in recent mass spectrometry (MS) experiments (*6*), it is supported by structural and genetic approaches (*12*, *17*, *18*). For example, T599 phosphorylation is mimicked by the most common oncogenic BRAF mutation, V600E, which generates a mutation-specific salt bridge between E600 and K507 in the αC helix of the N-lobe, which in turn shifts the αC helix and AS into the active "αC helix-IN/DFG-IN/R506-IN" conformation (*17*, *19*, *20*). Consequently, this salt bridge locks BRAF^{V600E} in the active conformation and exempts it from multiple regulatory requirements, including an intact RAS-binding domain, DIF, AS, and the C-terminal 14-3-3–binding site (*9*, *11*, *18*, *21*). The fact that BRAF^{V600E} can still provide high and transforming ERK activity in the presence of artificial DIF and/or C-terminal 14-3-3–binding site mutations suggests that it signals as a monomer, and indeed, it could be shown that it is only receptive to V600E-selective type I$^{1/2}$ RAF inhibitors (RAFi) in its monomeric state due to the phenomenon of negative allostery (*20*, *22*). However, these findings do not indicate that BRAF^{V600E} always exists as a monomer in living cells. We and others showed that BRAF^{V600E} displays a higher dimerization propensity than wild-type (WT) BRAF (BRAF^{WT}) and is more effective in phosphorylating MEK in its dimeric state and that a large fraction of this oncoprotein resides in large protein complexes that are sensitive to DIF mutations (*9*, *17*, *23*, *24*).

The phosphorylation- and dimerization-induced conformational changes within the kinase domain also promote its transition from an inactive to an active conformation, involving the realignment of conserved hydrophobic regulatory residues. If they are aligned in the active conformation, they will constitute the so-called R-spine that is essential for catalysis. The spine residues provide critical contact points for RAFi, and hence, their orientation, along with that of the αC helix and the AS, decides about drug binding and efficacy (*12*, *25*). For example, the clinically irrelevant type I inhibitors stabilize the RAF kinase domain in its active αC helix-in/DFG-in/R506in conformation, while type II compounds, such as the approved sorafenib and the clinical phase 2 trialed naporafenib, stabilize the αC helix-in/DFG-out/R506in conformation. The clinically used $BRAF^{V600E}$-selective drugs vemurafenib, dabrafenib, and encorafenib represent the aforementioned type $I^{1/2}$ inhibitors, inducing an αC-helix-out/DFG-in/R506in conformation (*20*).

The spectrum of *BRAF* alterations is still expanding because of the increasing sequence coverage of tumor genomes. Oncogenic mutations are subdivided into single-nucleotide/amino acid substitutions (e.g., V600E), small in-frame insertions/deletions resulting in full-length BRAF proteins with altered kinase activity, and gene fusions (*26*). Their complexity is increased by the fact that BRAF oncoproteins differ in their enzymatic activity and drive MEK/ERK hyperactivation by various mechanisms (*27*). These differences have practical implications for targeted therapies and stimulated the classification of BRAF oncoproteins (*26*). Class I mutants are confined to V600 substitutions and can still unfold their high intrinsic enzymatic activity and oncogenic signaling potential if deprived of the aforementioned dimer-promoting features. In contrast, class III mutants represent the other end of the spectrum as they display lower intrinsic kinase activity than $BRAF^{WT}$ or lack kinase activity at all. They cooperate with activated RAS and induce paradoxical MEK hyperactivation by dimerizing with catalytically competent RAF protomers and promoting their transactivation (*9*, *28*, *29*). Class II contains a wide spectrum of BRAF oncoproteins with varying degrees of intermediate activity (*30*). They rely on dimerization but can signal independent of RAS (*21*).

The so-called $BRAF^{\Delta\beta3\text{-}\alpha C}$ mutants represent still relatively underexplored but potentially highly active oncoproteins found in various tumor entities, especially in *KRAS* WT pancreatic neoplasia (*31*–*34*). According to the Catalogue Of Somatic Mutations In Cancer (COSMIC) database, 0.005% of its curated pan-cancer samples encode $BRAF^{\Delta\beta3\text{-}\alpha C}$ mutants. As the responsible mutations map to exon 12, which is ignored by most diagnostic procedures that only address exons 11 and 15, their frequency is probably underestimated, in particular for "*RAS/BRAF* WT" tumors of typically RAS/ERK pathway–driven entities. At the protein level, $BRAF^{\Delta\beta3\text{-}\alpha C}$ mutants are characterized by short in-frame deletions removing usually five amino acids in the loop linking the β3 strand with the αC helix (*35*–*37*). As this deletion affects the orientation of the αC helix (Fig. 1A), which in turn controls the exposure of the $R^{506}KTR^{509}HV$ motif, $BRAF^{\Delta\beta3\text{-}\alpha C}$ mutants might display an aberrant dimerization behavior. However, the first studies describing $BRAF^{\Delta\beta3\text{-}\alpha C}$ mutants arrived at different conclusions whether they signal as dimers or autonomous monomers (*35*–*37*). However, defining the biochemical properties of $BRAF^{\Delta\beta3\text{-}\alpha C}$ mutants, which determine RAFi efficacy, is of direct clinical relevance, as Molecular Tumor Boards (MTBs) increasingly discuss the druggability of these oncoproteins in clinical decision-making. Here, we provide an in-depth analysis of the signaling potential and dimerization state of various $BRAF^{\Delta\beta3\text{-}\alpha C}$ oncoproteins, including the previously uncharacterized $BRAF^{\Delta LNVTAP>F}$ oncoprotein and the hitherto undescribed $BRAF^{delinsFS}$ and $BRAF^{\Delta LNVT>F}$ mutants. By defining their druggability, we observed an unexpected variety in dabrafenib responsiveness, while sorafenib and the phase 2 trialed compound naporafenib inhibit all mutants tested. We also dissect the mechanism determining dabrafenib sensitivity and propose an algorithm for choosing the appropriate RAFi in the clinical setting.

RESULTS

Identification of the previously unidentified in-frame deletion mutant $BRAF^{delinsFS}$

This study was prompted by a pancreatic ductal adenocarcinoma (PDAC) case analyzed within the Molecularly Aided Stratification for Tumor Eradication Research (MASTER) program of the National Center for Tumor Diseases (NCT) and the German Cancer Consortium (DKTK) (*38*) in which a BRAF exon 12 p.L485-P490delinsFS ($BRAF^{delinsFS}$) was detected. The patient was diagnosed with poorly differentiated PDAC and hepatic metastases at

[1]Institute of Molecular Medicine, ZBMZ, Faculty of Medicine, University of Freiburg, 79104 Freiburg, Germany. [2]Faculty of Biology, University of Freiburg, Freiburg, Germany. [3]German Cancer Consortium (DKTK), partner site Freiburg and German Cancer Research Center (DKFZ), 69120 Heidelberg, Germany. [4]Freeze-O Organoid Bank, University Medical Center, Faculty of Medicine, University of Freiburg, Freiburg, Germany. [5]Department of Internal Medicine I (Hematology, Oncology, and Stem Cell Transplantation), University Hospital of Freiburg, Freiburg, Germany. [6]Institute of Medical Bioinformatics and Systems Medicine (IBSM), Freiburg University Medical Center, Faculty of Medicine, University of Freiburg, Freiburg, Germany. [7]Department of Biology, University of Fribourg, 1700 Fribourg, Switzerland. [8]Division of Translational Medical Oncology, National Center for Tumor Diseases (NCT) Heidelberg and German Cancer Research Center (DKFZ), 69120 Heidelberg, Germany. [9]German Cancer Consortium (DKTK), Heidelberg, Germany. [10]PanCuRx Translational Research Initiative, Ontario Institute for Cancer Research, Toronto, Ontario, Canada. [11]Princess Margaret Cancer Centre, University Health Network, Toronto, Ontario, Canada. [12]Department of Dermatology, University Hospital of Tübingen, Tübingen, Germany. [13]German Cancer Consortium (DKTK), DKFZ partner site Tübingen, Eberhard Karls University, Tübingen, Germany. [14]Center for Personalized Medicine Tübingen, Eberhard Karls University, Tübingen, Germany. [15]Department of Internal Medicine I, Eberhard-Karls University, Tübingen, Germany. [16]Department of General and Visceral Surgery, University of Freiburg Medical Center, Faculty of Medicine, 79106 Freiburg, Germany. [17]Comprehensive Cancer Center Freiburg (CCCF), Medical Center, Faculty of Medicine, University of Freiburg, 79106 Freiburg, Germany. [18]Department for Translational Medical Oncology, National Center for Tumor Diseases (NCT/UCC), Dresden, Germany. [19]German Cancer Research Center (DKFZ), Heidelberg, Germany. [20]Faculty of Medicine and University Hospital Carl Gustav Carus, Technische Universität Dresden, Dresden, Germany. [21]Helmholtz-Zentrum Dresden–Rossendorf (HZDR), Dresden, Germany. [22]Translational Medical Oncology, Faculty of Medicine and University Hospital Carl Gustav Carus, Technische Universität Dresden, Dresden, Germany. [23]German Cancer Consortium (DKTK), Dresden, Germany. [24]Technische Universität Dresden, Faculty of Biology, Technische Universität Dresden, Dresden, Germany. [25]Translational Functional Cancer Genomics, National Center for Tumor Diseases (NCT) and German Cancer Research Center (DKFZ), Heidelberg, Germany. [26]Computational Oncology Group, Molecular Precision Oncology Program, National Center for Tumor Diseases (NCT) Heidelberg and German Cancer Research Center (DKFZ), Heidelberg, Germany. [27]Pattern Recognition and Digital Medicine Group, Heidelberg Institute for Stem Cell Technology and Experimental Medicine (HI-STEM), Heidelberg, Germany. [28]Department of Medical Oncology and Haematology, University Hospital of Zurich, Zurich, Switzerland. [29]Center for Biological Signalling Studies BIOSS, University of Freiburg, 79104 Freiburg, Germany.
*Corresponding author. Email: tilman.brummer@mol-med.uni-freiburg.de

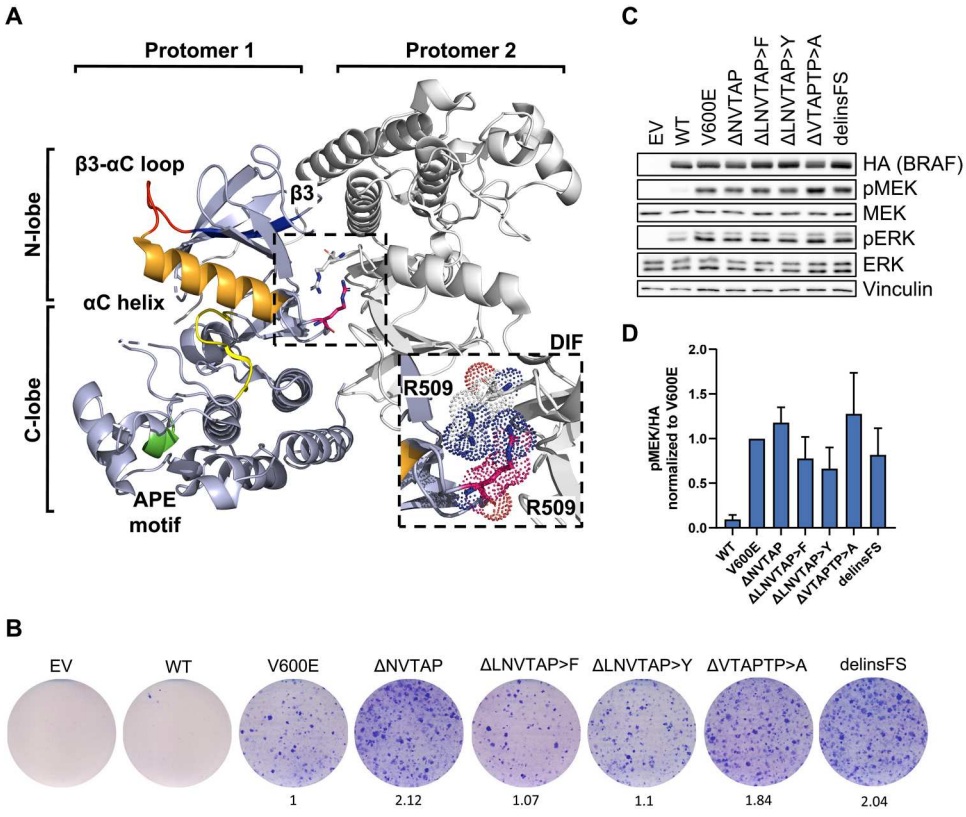


Fig. 1. The recently identified Δβ3-αC mutation BRAF^{delinsFS} is activating and confers transforming ability. (**A**) BRAF elements that are essential in this study are highlighted in protomer 1 of a representative BRAF dimer. Orange, αC helix; red, αC-β3 loop; blue, β3 sheet; pink, R509; green, APE motif; yellow, D^{594}FGLATV^{600}KS motif of the AS. The ribbon diagram, which is based on a crystal structure of dimerized human BRAF kinase domains bound to 14-3-3 proteins [PDB: 6XAG, (*113*)], was created using the PyMol Molecular Graphics System (version 2.5.2, Schrödinger, LLC). The 14-3-3 dimer was excluded for simplicity. (**B**) Focus formation assay. MEFs were infected with retroviral vectors encoding the indicated BRAF proteins, cultured for 14 days, and stained with Giemsa reagent. To quantify focus formation, the integrated pixel density was determined using ImageJ and normalized to BRAF^{V600E}. (**C**) Immunoblot of HEK293T cells expressing the indicated BRAF proteins. (**D**) Immunoblots were quantified using ImageJ. The bar graph shows pMEK/hemagglutinin (HA) levels (means + SD, *n* = 3) normalized to BRAF^{V600E}. Images are representative of at least three independent experiments.

the age of 58. Palliative chemotherapy with mFOLFIRINOX [oxaliplatin, leucovorin, irinotecan, and 5-fluorouracil (5-FU)] resulted in an objective response and was deescalated to 5-FU after 7 months. At disease progression 4 months later, treatment was changed to irinotecan/5-FU [time to progression (TTP), 6 months]. Further treatment lines were nab-paclitaxel/gemcitabine (TTP, 7 months), nal-irinotecan (TTP, 9 months), and FOLFOX4 (TTP, 2 months). The patient was then enrolled in NCT/DKTK MASTER, and treatment was switched to gemcitabine/erlotinib (TTP, 3 months), which was continued beyond progression due to reduced tumor growth compared to previous regimens and a lack of therapeutic alternatives. On the basis of the BRAF^{delinsFS} mutation detected, MEK inhibition ± RAFi was recommended by the MTB. Unfortunately, no suitable clinical trial was available at that time, and the patient died 3 months later at the age of 62.

BRAF^{delinsFS} lacks six of the original amino acids of the β3-αC helix loop but carries two de novo–introduced residues, a phenylalanine and a serine, in this segment (Fig. 1A). As this represents a net deletion of four amino acids, as compared to the previously published Δβ3-αC mutants, and because deletion length influences signaling activity (*36*, *37*), we analyzed the properties of BRAF^{delinsFS}. First, we compared the transformation potential of the previously uncharacterized BRAF^{delinsFS} mutant with that of other Δβ3-αC mutants (described in fig. S1) and BRAF^{V600E} in immortalized murine embryonic fibroblasts (MEFs) (Fig. 1B). BRAF^{delinsFS} induces foci to a similar extent as the other Δβ3-αC mutants, including the previously described but functionally uncharacterized BRAF$^{\Delta LNVTAP>F}$ (*39*). Commensurate with their transformation potential, all mutants activated the ERK pathway in human embryonic kidney (HEK) 293T cells (Fig. 1, C and D). The MEK/ERK phosphorylation potential of BRAF$^{\Delta\beta3\text{-}\alpha C}$ mutants was not affected by the AVKA mutation replacing T599 and S602 by alanine residues (fig. S1B). This is reminiscent of BRAF^{V600E}, which, unlike other BRAF oncoproteins, signals independent of an intact T^{599}V^{600}KS^{602} motif (*18*, *40*, *41*), indicating that AS-induced conformational changes are also dispensable for BRAF$^{\Delta\beta3\text{-}\alpha C}$ oncoproteins.

BRAF$^{\Delta\beta3\text{-}\alpha C}$ mutants require dimerization for oncogenic signaling and stability

The initial studies disagreed whether BRAF$^{\Delta\beta3\text{-}\alpha C}$ act as mono- or dimers and whether they require an intact DIF to unfold their oncogenic potential (*24*, *35*, *36*). This discrepancy could be explained by the fact that these laboratories studied different BRAF$^{\Delta\beta3\text{-}\alpha C}$ mutants (fig. S1A). Therefore, we assessed the dimerization capacity

of BRAF^{delinsFS}, which formed heterodimers with RAF1 and displayed increased homodimerization potential with coexpressed BRAF^{WT} and even more pronounced with itself (fig. S1C). This finding and the aforementioned controversy about the requirements of BRAF$^{\Delta\beta3\text{-}\alpha C}$ mutants for an intact DIF prompted us to systematically analyze the effects of the R509H and AAE mutations, either singly or in combination, on the signaling potential of these oncoproteins (Fig. 2). The typical DIF mutation, R509H, impairs BRAF homo- and, albeit to a lesser extent, heterodimerization (*9*). The AAE mutation was inspired by the noncanonical APE motif (AAE) at the C-terminal end of the ARAF AS that indirectly decreases the dimerization propensity of RAF kinases (*24*). We included BRAF^{V600E} as a reference for a BRAF oncoprotein that can signal and transform independent of an intact DIF (*9*, *11*, *24*, *42*). Commensurate with previous findings (*9*, *24*), the R509H and AAE substitutions had a strong and severe impact on the MEK phosphorylation potential of BRAF^{WT}, respectively. In contrast, BRAF^{V600E} was less affected and only the simultaneous introduction of the R509H and AAE mutations reduced the MEK phosphorylation potential by more than 50% (Fig. 2B). Likewise, the BRAF$^{\Delta\beta3\text{-}\alpha C}$ mutants resembled BRAF^{V600E} as they remained highly and moderately active in the presence of the R509H and AAE alterations, respectively. Only their combination reduced the MEK phosphorylation potential of BRAF^{V600E} by more than 70%. Unexpectedly, the BRAF$^{\Delta\beta3\text{-}\alpha C}$ mutants differed in their sensitivity toward the R509H and AAE mutations, with BRAF$^{\Delta LNVTAP>F}$ and BRAF$^{\Delta LNVTAP>Y}$ being most resistant (Fig. 2, A and B).

We also assessed the transformation potential of the BRAF$^{\Delta\beta3\text{-}\alpha C}$ mutants in simian virus 40 large T antigen immortalized murine fibroblasts (MEFs) and compared it with that of BRAF^{V600E} and BRAF^{F595L}, another oncoprotein with lower intrinsic kinase activity than BRAF^{V600E} (*43*) but potent focus formation potential (*44*).

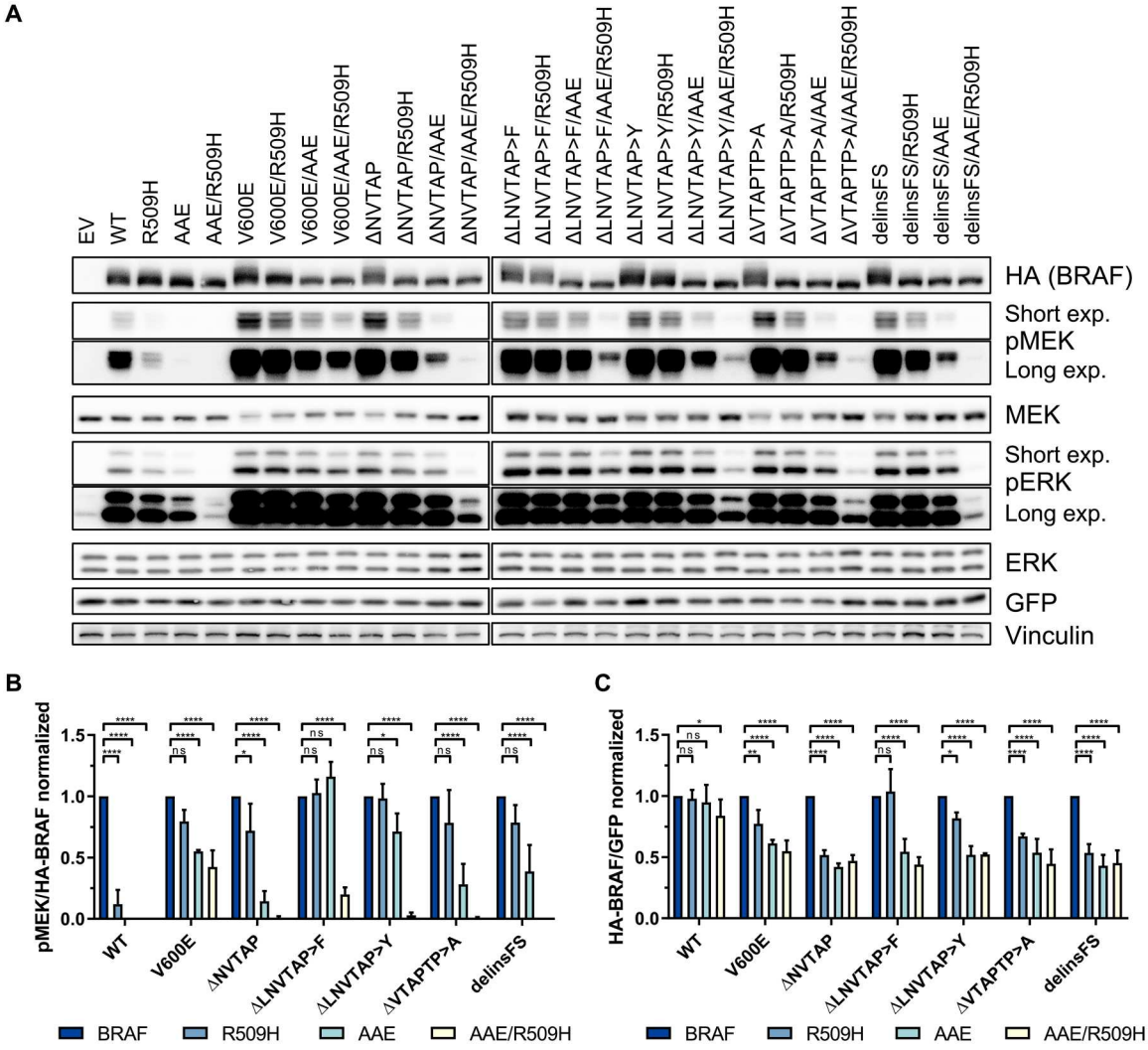


Fig. 2. Dimerization is essential for the activity and stability of BRAF$^{\Delta\beta3\text{-}\alpha C}$ mutants. (**A**) HEK293T cells were transiently transfected with the indicated HA-BRAF plasmids. Total cell lysates (TCLs) were analyzed by immunoblot using the indicated antibodies. Vinculin detection serves as a loading control. Images are representative of three independent experiments. (**B** and **C**) Immunoblots were quantified using ImageJ. Data were normalized to the corresponding BRAF protein without the additional dimerization-impairing mutations R509H and/or AAE. Statistical analysis: means + SD, $n = 3$, two-way analysis of variance (ANOVA) with Dunnett's test for multiple comparisons, $^{*}P \leq 0.05$, $^{**}P \leq 0.01$, $^{***}P \leq 0.001$, $^{****}P \leq 0.0001$. ns, not significant.

These MEFs display a stringent contact inhibition response that is only overridden by oncogenic but not WT BRAF (*18*, *40*, *44*). As seen in Fig. 1B and fig. S2A, all $BRAF^{\Delta\beta3\text{-}\alpha C}$ mutants caused focus formation to a similar extent as the high-intensity $BRAF^{V600E}$ mutant, and hence, their transforming activity correlates with their MEK phosphorylation potential. However, introducing the R509H and AAE mutations, either singly or in combination, increased the focus formation of MEFs transformed by $BRAF^{\Delta\beta3\text{-}\alpha C}$ mutants, albeit this effect was influenced by the individual in-frame deletion. At first glance, this observation appears counterintuitive but ties in with our previous observation that BRAF oncoproteins with an intermediate activity, e.g., $BRAF^{F595L}$, are more effective in driving the proliferation of these MEFs than $BRAF^{V600E}$ (*18*, *44*). Thus, although all cells expressing $BRAF^{V600E}$ and the $BRAF^{\Delta\beta3\text{-}\alpha C}$ mutants displayed a transformed morphology (fig. S2B), the correlation between MEK/ERK phosphorylation and focus proliferation follows a bell-shape curve (fig. S2C).

The R509H and AAE mutations increased the electrophoretic mobility of all BRAF proteins, which probably reflects their decreased phosphorylation status due to reduced feedback and trans-phosphorylation events (*45*). On closer inspection of the BRAF bands on well-resolved Western blots (Fig. 2A), we noticed that R509H and, in particular, AAE reduced the amount of the BRAF proteins. This apparent reduction was not caused by differences in phosphorylation status that might interfere with protein transfer or detection, as dephosphorylation of $BRAF^{\Delta NVTAP}$ did not increase its abundance (fig. S3). To distinguish between an effect on BRAF stability and abundance differences caused by distinct transfection efficiencies or transcript production/stability, we exploited the bicistronic design of the hemagglutinin (HA)–BRAF–internal ribosomal entry site (IRES)–green fluorescent protein (GFP) cassette of the pMIG vectors from which HA-BRAF and GFP are coexpressed (*9*). The quantitative assessment of the HA-BRAF/GFP ratio confirmed that $BRAF^{WT}$ levels were hardly affected by dimerization-impairing mutations (Fig. 2C). R509H had little to no effects on the abundance of the high-activity $BRAF^{V600E}$ class I mutant, the intermediate-activity class II mutant $BRAF^{F595L}$ (*44*), $BRAF^{\Delta LNVTAP>F}$, and $BRAF^{\Delta LNVTAP>Y}$, while that of the other $BRAF^{\Delta\beta3\text{-}\alpha C}$ mutants was reduced by 30 to 50% (Fig. 2, A and C, and fig. S4, A and C). Linear regression between GFP-normalized HA-BRAF expression and HA-BRAF–normalized pMEK levels upon R509H introduction revealed that, in contrast to the class II mutant $BRAF^{F595L}$, the stability of $BRAF^{\Delta\beta3\text{-}\alpha C}$ mutants, as reflected by their abundance, correlates with their MEK phosphorylation potential (fig. S4, B to D). It should be noted that the effects of the R509H and AAE mutations on the stability of $BRAF^{\Delta\beta3\text{-}\alpha C}$ mutants were neither quantified nor remarked in the initial publications (*24*, *35*, *36*). Upon densitometry of the Western blot bands in these three publications, however, we noted that all three studies showed that the R509H mutation reduced the abundance of all $BRAF^{\Delta\beta3\text{-}\alpha C}$ mutants to a similar extent (fig. S4E).

$BRAF^{\Delta\beta3\text{-}\alpha C}$ mutants display high dimerization propensity and form large multiprotein complexes containing heat shock protein 90

Given the profound effect of dimer impairing mutations on the activity and stability of $BRAF^{\Delta\beta3\text{-}\alpha C}$ mutants, we next analyzed their homodimerization potential (Fig. 3, A and B). This experimental setup in which the BRAF dimers are purified by anti-HA immunoprecipitation reveals stable dimers and can discriminate the various affinities displayed by BRAF mutants. Using this assay, we, and subsequently others applying different methods, demonstrated that $BRAF^{V600E}$, despite its ability to signal as a monomer under artificial circumstances, has a higher homodimerization propensity than $BRAF^{WT}$ (*9*, *17*, *46*). Unexpectedly, all $BRAF^{\Delta\beta3\text{-}\alpha C}$ mutants displayed an even higher and significantly elevated homodimerization potential compared to $BRAF^{V600E}$ (Fig. 3, A and B). Nevertheless, homodimerization was reduced but not abolished by the R509H mutation, whereas combination of R509H and AAE mutations abrogated the homodimerization potential of all analyzed mutants. The $BRAF^{\Delta LNVTAP>F}$ oncoprotein, whose MEK/ERK phosphorylation potential was the least affected by the R509H substitution, still retained more than fivefold homodimerization capacity over $BRAF^{V600E}$ after introducing this DIF mutation.

Almost all high-activity BRAF point mutants, except for a few variants such as the highly dimerization-proficient $BRAF^{E585K}$ oncoprotein, require the heat shock protein 90 (HSP90)/CDC37 chaperone complex for their activity (*47*, *48*). In addition, $BRAF^{V600E}$ forms large multiprotein complexes with this chaperone (*23*). As the requirement and affinity of $BRAF^{\Delta\beta3\text{-}\alpha C}$ mutants for HSP90 remains unknown, we assessed the HSP90 levels in immunoprecipitates and observed increased HSP90 binding compared to $BRAF^{WT}$, albeit to a different extent (Fig. 3, A, C, and D). The only exception is $BRAF^{\Delta LNVTAP>F}$, which exhibits no significant difference in HSP90 recruitment compared to $BRAF^{WT}$. The dimerization impairing R509H and AAE mutations further increased the interaction between HSP90 and the various $BRAF^{\Delta\beta3\text{-}\alpha C}$ mutants. Nonlinear regression of precipitated $BRAF^{\Delta\beta3\text{-}\alpha C}$ mutants and HSP90 revealed a negative correlation among $BRAF^{\Delta\beta3\text{-}\alpha C}$ mutants between homodimerization and HSP90 binding (fig. S5A), suggesting that dimerization and HSP90 binding cooperate and potentially compensate each other in stabilizing $BRAF^{\Delta\beta3\text{-}\alpha C}$ mutants. Using blue native polyacrylamide gel electrophoresis (BN-PAGE) and size exclusion chromatography–based proteomics, we demonstrated previously that hyperactive and dimeric $BRAF^{V600E}$ predominantly occurs in a large multiprotein complex enriched with HSP90 and its co-chaperone CDC37, while $BRAF^{WT}$ is mostly confined to a small complex (*9*, *23*). Therefore, we applied BN-PAGE to compare the sizes of multiprotein complexes containing either $BRAF^{WT}$, $BRAF^{V600E}$, $BRAF^{\Delta NVTAP}$, or $BRAF^{\Delta LNVTAP>F}$. This analysis revealed that the propensity of $BRAF^{V600E}$ to form a large multiprotein complex was even further enhanced in both $BRAF^{\Delta\beta3\text{-}\alpha C}$ mutants, as the small complex almost completely disappeared in these samples (Fig. 3E and fig. S5B). This effect was most pronounced in lysates from cells expressing $BRAF^{\Delta LNVTAP>F}$, which displayed a particularly large complex of >880 kDa. Albeit to a lesser extent, this complex was also observed in lysates from $BRAF^{\Delta NVTAP}$ but not detected in those expressing $BRAF^{V600E}$ or $BRAF^{WT}$. The increasing abundance in large BRAF complexes and the emergence of the >880 kDa complex correlate with the strongly increased dimerization potential of both $BRAF^{\Delta\beta3\text{-}\alpha C}$ mutants compared to $BRAF^{V600E}$ (Fig. 3B). Given the unexpected finding that $BRAF^{\Delta LNVTAP>F}$, unlike the other $BRAF^{\Delta\beta3\text{-}\alpha C}$ mutants, did not differ from $BRAF^{WT}$ in terms of HSP90 recruitment (Fig. 3, A, C, and D), we analyzed the colocalization between BRAF, CDC37, and HSP90 in BN-PAGE experiments and the association of the three proteins by coimmunoprecipitation

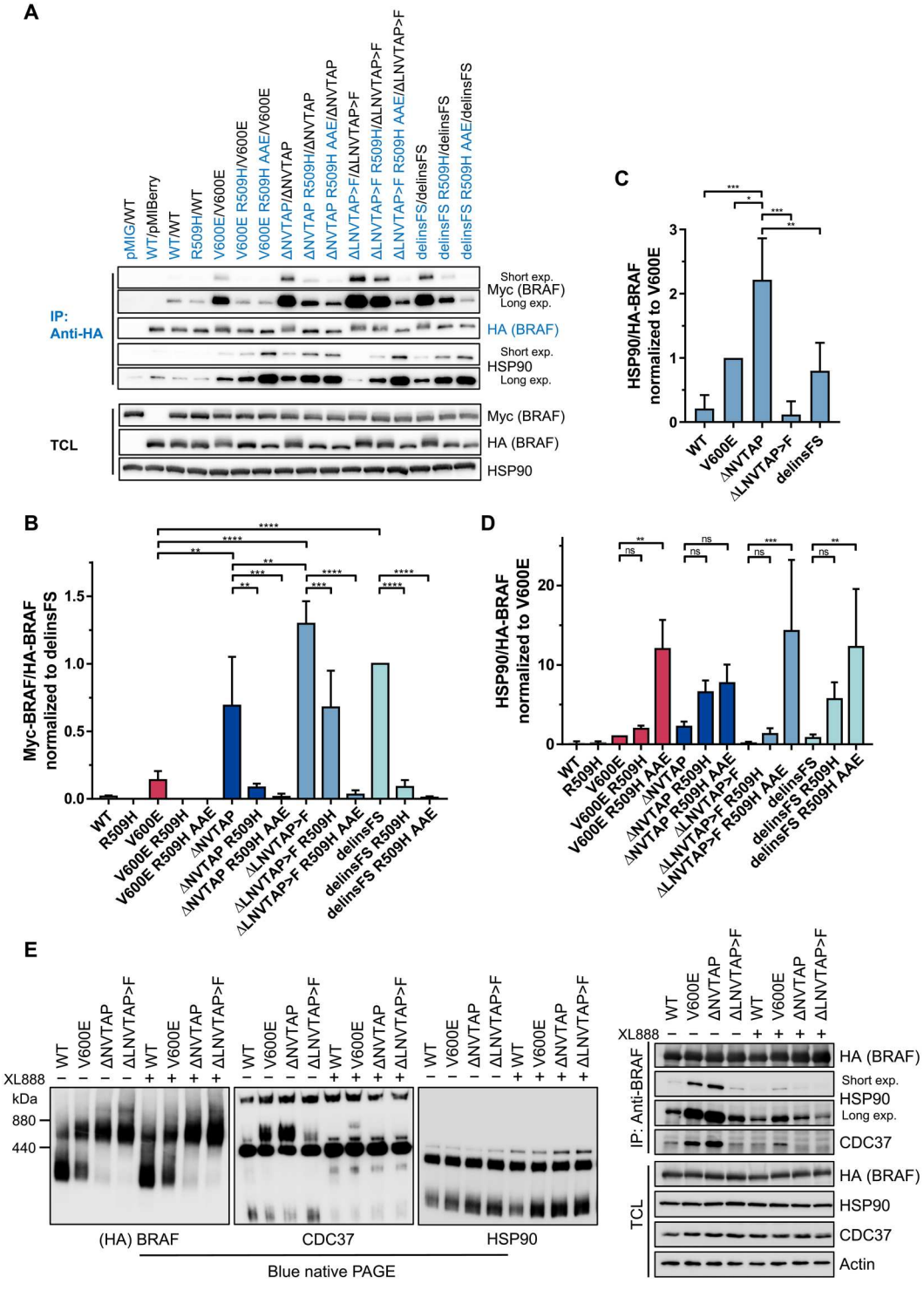


Fig. 3. BRAF$^{\Delta\beta3\text{-}\alpha C}$ mutants form exceptionally stable dimers, with varying sensitivities to the R509H mutation and affinity toward each other and heat shock protein 90. (**A**) The indicated HA- or Myc-tagged BRAF proteins were coexpressed in HEK293T cells. BRAF complexes were precipitated with an anti-HA antibody. Immunoprecipitates and TCLs were analyzed by immunoblot using the indicated antibodies. TCLs confirm the expression of heat shock protein 90 (HSP90) and the BRAF proteins in question for all coimmunoprecipitations. Images are representative of three independent experiments. IP, immunoprecipitation. (**B** to **D**) Immunoblots were quantified using ImageJ. Bar graphs show copurified Myc-BRAF (B) or HSP90 [(C) and (D)] per precipitated HA-BRAF. Statistical analysis: means + SD, $n = 3$, one-way (C) or two-way [(B) and (D)] ANOVA with Tukey's [(B) and (C)] or Dunnett's (D) test for multiple comparisons, $^{*}P \leq 0.05$, $^{**}P \leq 0.01$, $^{***}P \leq 0.001$, $^{****}P \leq 0.0001$. (**E**) Analysis of BRAF complexes by BN-PAGE. HEK293T cells expressing the indicated BRAF proteins were cultured in the presence of the HSP90 inhibitor XL888 (1 μM) or vehicle control for 4 hours, followed by lysis. TCLs were analyzed by Western blotting following BN-PAGE (left), using the indicated antibodies. To confirm the inhibition of HSP90 binding, BRAF complexes were precipitated using an anti-HA antibody, followed by SDS-PAGE and Western blotting. TCLs confirm comparable expression levels of CDC37, HSP90, and the BRAF proteins in question for coimmunoprecipitation and BN-PAGE. Representative images for two biological replicates are shown. See also fig. S5B.

(Fig. 3E). CDC37, which recruits kinases to HSP90, was enriched in large complexes comigrating with that of BRAF^{V600E} and BRAF$^{\Delta NVTAP}$, and this colocalization was almost abolished by the clinically tested HSP90 inhibitor XL888 (*49*). As expected from the coimmunoprecipitation experiments shown in Fig. 3 (A, C, and D), CDC37 was less abundant in large complexes comigrating with those organized by BRAF$^{\Delta LNVTAP>F}$. Unfortunately, we could not identify an HSP90 complex that comigrated with the large BRAF-containing complexes in our BN-PAGE experiments. We assume that the epitope for the anti-HSP90 antibody is not accessible in native complexes because HSP90 and CDC37 were readily detected as XL888-sensitive interactors in SDS-PAGE–resolved and, hence, denatured BRAF^{V600E} and BRAF$^{\Delta NVTAP}$ coimmunoprecipitates from this experimental setup (Fig. 3E).

Together, our BN-PAGE and coimmunoprecipitation experiments indicate that the CDC37/HSP90 complex is present in the large molecular mass complexes typically formed by $BRAF^{V600E}$ and $BRAF^{\Delta NVTAP}$ but not $BRAF^{\Delta LNVTAP>F}$. Our data also show that BRAF oncoproteins do not form one but multiple high molecular mass complexes and that the >880 kDa complex observed predominantly in $BRAF^{\Delta LNVTAP>F}$-expressing cells predicts a multiprotein assembly independent of HSP90/CDC37.

Vulnerability of $BRAF^{\Delta\beta3\text{-}\alpha C}$ mutants toward HSP90 inhibition correlates with their dimerization propensity

The reduced abundance of $BRAF^{\Delta\beta3\text{-}\alpha C}$ mutants could be linked to an inherent instability that is compensated by increased homodimerization and/or HSP90 binding. To address these hypotheses, we generated *Braf*-deficient MEFs harboring tetracycline (tet)–regulated expression vectors for the BRAF proteins in question to monitor their longevity following tet washout (fig. S6). $BRAF^{WT}$, its R509H/AAE counterpart, and $BRAF^{\Delta LNVTAP>F}$ displayed longer half-lives than $BRAF^{\Delta NVTAP}$ and $BRAF^{V600E}$ (fig. S6, A to C). Our calculated half-life of $BRAF^{V600E}$ in MEFs was in a similar range as reported for HEK293T cells (*50*). In agreement with the reduced BRAF levels shown in Fig. 2, impairing the dimerization potential of $BRAF^{\Delta LNVTAP>F}$ by the R509H/AAE mutations reduced its half-life into the range of $BRAF^{\Delta NVTAP}$ and $BRAF^{V600E}$ (fig. S6C).

Next, we investigated whether XL888 would affect the stability of $BRAF^{\Delta\beta3\text{-}\alpha C}$ oncoproteins (Fig. 4, A and B, and fig. S7). XL888 caused a noticeable depletion of $BRAF^{\Delta NVTAP}$ down to 50%. In contrast, $BRAF^{\Delta LNVTAP>F}$ levels were only mildly reduced at 8 hours and comparable to those of $BRAF^{WT}$. In line with Fig. 3, increased HSP90 binding induced by reduction of dimerization potential (R509H AAE) sensitized $BRAF^{\Delta LNVTAP>F}$ and $BRAF^{WT}$ for HSP90 inhibition. This suggests that $BRAF^{\Delta\beta3\text{-}\alpha C}$ mutants are less stable and are stabilized to a different extent by increased dimerization or HSP90 binding.

To confirm the decreased stability and enhanced XL888 sensitivity of an endogenously expressed $BRAF^{\Delta\beta3\text{-}\alpha C}$ mutant, we established an approach using the human ovarian carcinoma cell line OV-90 in which we can monitor the coexpression, as suggested by genomic polymerase chain reaction (PCR) (fig. S13A), and abundance of $BRAF^{WT}$ and $BRAF^{\Delta NVTAP}$ side by side. By looking at the distribution of trypsin cleavage sites in BRAF, we reasoned not only that MS would allow us to detect a peptide specific for the ΔNVTAP deletion but also that HSP90 inhibition should trigger its depletion. The $BRAF^{\Delta NVTAP}$-derived peptide was reduced by 50% upon XL888 treatment, whereas the abundance of the $BRAF^{WT}$ peptide was unaffected (Fig. 4C). Our MS approach might be also of diagnostic interest as it could be useful to confirm the endogenous expression of similar oncoproteins generated by short in-frame deletions/insertions, e.g., epidermal growth factor receptor (EGFR) and HER2 (*36*), which cannot easily be distinguished from their WT counterparts by Western blotting or by immunohistochemistry.

$BRAF^{\Delta\beta3\text{-}\alpha C}$ mutants differ in their sensitivity toward type $I^{1/2}$ inhibitors but are all blocked by type II compounds

However, how could tumors with $BRAF^{\Delta\beta3\text{-}\alpha C}$ mutants be treated with targeted therapy? MEK inhibitors (MEKi) would be an obvious choice as trametinib blocked ERK pathway activation by all $BRAF^{\Delta\beta3\text{-}\alpha C}$ oncoproteins (fig. S8A). We also searched for a strategy directly inhibiting $BRAF^{\Delta\beta3\text{-}\alpha C}$ mutants as such a RAFi could be very useful, either in a monotherapy setting or as a component of a vertical pathway inhibition strategy (*51*). In the initial studies, however, the tested $BRAF^{\Delta\beta3\text{-}\alpha C}$ mutants were not blocked by the type $I^{1/2}$ inhibitor vemurafenib, while they remained sensitive toward the type I inhibitor GDC-0879 and the type II inhibitors LY3009120 and AZ-628 (*35*, *36*). We confirmed these findings for LY30009120 and vemurafenib and extended them to other $BRAF^{\Delta\beta3\text{-}\alpha C}$ mutants (fig. S8, B and C).

As the phase 1 trial of LY3009120 was terminated because of inefficacy (*52*) and GDC-0879 as well as AZ-628 have not progressed beyond preclinical testing [(*19*) and our own research on https://clinicaltrials.gov], we first analyzed the sensitivity of the highly active and dimerizing $BRAF^{\Delta LNVTAP>F}$ oncoprotein toward other type II inhibitors, including the clinically applied sorafenib and currently trialed inhibitors such as belvarafenib (*53*) and naporafenib (LXH254) (*54*). We also tested the clinically available type $I^{1/2}$ inhibitors dabrafenib and encorafenib for their activity against $BRAF^{\Delta LNVTAP>F}$. While few data are available for dabrafenib for $BRAF^{\Delta NVTAP}$ (*35*), the activity of encorafenib against $BRAF^{\Delta\beta3\text{-}\alpha C}$ mutants is unknown. Both type $I^{1/2}$ inhibitors were ineffective against $BRAF^{\Delta LNVTAP>F}$ (fig. S8D). In contrast, all type II inhibitors impaired MEK/ERK activation by $BRAF^{\Delta LNVTAP>F}$.

Given the poor sensitivity of $BRAF^{\Delta\beta3\text{-}\alpha C}$ mutants toward vemurafenib (fig. S8C), the clinical availability of dabrafenib and encorafenib, and their distinct effects on kinase domain conformation (*19*), we compared the sensitivity of additional in-frame deletion mutants to these type $I^{1/2}$ inhibitors and naporafenib. HEK293T cells expressing $BRAF^{V600E}$ served as reference for successful inhibition by dabrafenib and encorafenib. While encorafenib was quite ineffective in reducing MEK phosphorylation triggered by all $BRAF^{\Delta\beta3\text{-}\alpha C}$ mutants, dabrafenib inhibited $BRAF^{\Delta NVTAP}$ and $BRAF^{\Delta VTAPTP>A}$ but not $BRAF^{\Delta LNVTAP>F}$, $BRAF^{\Delta LNVTAP>Y}$, and $BRAF^{delinsFS}$. Notably, we rather observed a trend for increased MEK phosphorylation in cells expressing $BRAF^{\Delta LNVTAP>F}$ and $BRAF^{\Delta LNVTAP>Y}$ treated with these type $I^{1/2}$ inhibitors (Fig. 5, A, B, E, and F). In contrast, the type II inhibitor naporafenib was effective against all $BRAF^{\Delta\beta3\text{-}\alpha C}$ mutants (Fig. 5, C to G). As often observed in these experiments and probably reflecting the multiple feedback loops and rheostasis mechanisms operating in the RAS/ERK pathway (*40*, *55*–*58*), the RAFi-mediated effects were more pronounced at the level of MEK than ERK phosphorylation. Nevertheless, pERK levels followed similar trends (fig. S9).

Given the contrasting efficacies of type $I^{1/2}$ compounds against the various $BRAF^{\Delta\beta3\text{-}\alpha C}$ mutants, we next assessed their affinity in a cellular thermal shift assay (CETSA) in which drugs stabilize their target against heat-induced denaturation in cellulo (*59*). Thermal stability of the dabrafenib-sensitive mutants $BRAF^{\Delta NVTAP}$ and $BRAF^{V600E}$ (positive control) was increased by dabrafenib, whereas that of the insensitive $BRAF^{\Delta LNVTAP>F}$ oncoprotein remained unaffected, indicating inefficient drug accommodation (fig. S10, A to D). Thus, CETSA confirms the suspected variation in binding efficiency of dabrafenib to $BRAF^{\Delta\beta3\text{-}\alpha C}$ oncoproteins. $BRAF^{\Delta LNVTAP>F}$ activity, monitored via phospho-MEK levels (fig. S10E), was eventually inhibited in the presence of 100 μM dabrafenib, an exceptionally high concentration not achievable in a therapeutic setting, suggesting that drug binding to $BRAF^{\Delta LNVTAP>F}$ is not completely prevented. This impaired drug binding could explain the observed paradoxical activation in $BRAF^{\Delta LNVTAP>F}$- and $BRAF^{\Delta LNVTAP>Y}$-expressing HEK293T cells treated with

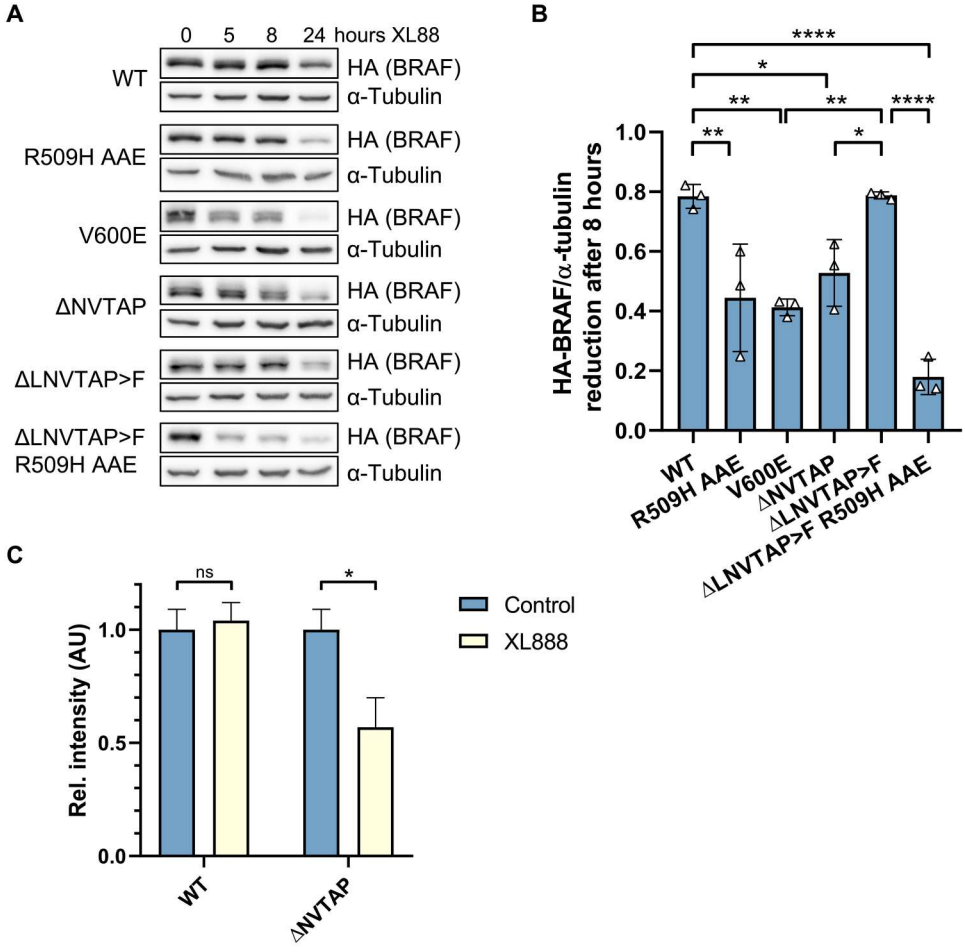


Fig. 4. BRAF$^{\Delta\beta3\text{-}\alpha C}$ mutants show enhanced susceptibility to HSP90 inhibition. (**A**) Expression of the indicated BRAF proteins in lentivirally transduced MEF lines was induced by tet addition for 72 hours, followed by addition of XL888 (1 μM). Cells were lysed after the indicated XL888 treatment periods, and HA-BRAF levels were quantified by Western blot. (**B**) BRAF levels were normalized to α-tubulin. Bar graph shows the reduction of BRAF levels after 8 hours. Statistical analysis: means + SD, $n = 3$, one-way ANOVA with Tukey's test for multiple comparisons, $^*P \leq 0.05$, $^{**}P \leq 0.01$, $^{***}P \leq 0.001$, $^{****}P \leq 0.0001$. (**C**) Following cultivation of OV-90 cells in the presence of 1 μM XL888 or control [dimethyl sulfoxide (DMSO)] for 24 hours, endogenous BRAF was purified and digested with trypsin before MS. Abundances of the BRAF^{WT} (MLNVTAPTPQQLQAFK)– and corresponding BRAF$^{\Delta NVTAP}$ (MLTPQQLQAFK)–derived peptides were compared between control (DMSO) and XL888-treated cells. Peptide abundance for both proteins purified from DMSO-treated cells was set to 1 and was measured in technical triplicates. Statistical analysis: means + SEM, unpaired, two-tailed *t* tests, $^*P \leq 0.05$, $^{**}P \leq 0.01$, $^{***}P \leq 0.001$, $^{****}P \leq 0.0001$. AU, arbitrary units.

encorafenib or dabrafenib (Fig. 5, A, B, D, and E). In cells expressing dabrafenib-/encorafenib-receptive mutants like BRAF$^{\Delta NVTAP}$, the applied inhibitor concentration saturated most protomers. In contrast, the same concentration is only subsaturating in cells expressing variants like BRAF$^{\Delta LNVTAP>F}$ and BRAF$^{\Delta LNVTAP>Y}$ that display a reduced binding affinity to these type $I^{1/2}$ compounds. The few drug-bound BRAF$^{\Delta LNVTAP>F/Y}$ protomers, however, that manage to take up these inhibitors might serve, because of their high dimerization propensity (Fig. 3B), as highly potent allosteric transactivators of drug-free RAF protomers, resulting in paradoxical MEK phosphorylation (*60*, *61*). This model is supported by Yuan *et al.* (*24*), showing that other BRAF$^{\Delta\beta3\text{-}\alpha C}$ oncoproteins rendered kinase-inactive by mutation serve as allosteric transactivators. Alternatively, but not excluding the first model, it might be possible that BRAF$^{\Delta LNVTAP>F}$ and BRAF$^{\Delta LNVTAP>Y}$, which are less likely occupied by type $I^{1/2}$ compounds, are further activated by drug-bound WT BRAF or RAF1, as both isoforms take up dabrafenib and encorafenib in the single-digit nanomolar range (*62*–*64*).

Next, we asked whether the high homodimerization propensity of BRAF$^{\Delta LNVTAP>F}$ could explain its dabrafenib resistance by negative allostery (*19*, *65*) and introduced the R509H mutation, either singly or in combination with the AAE substitution, into this oncoprotein. Unexpectedly, these alterations did not restore dabrafenib sensitivity, suggesting that other mechanisms modulate dabrafenib affinity of BRAF$^{\Delta\beta3\text{-}\alpha C}$ mutants (fig. S11).

In search of an explanation for the varying properties of the analyzed BRAF$^{\Delta\beta3\text{-}\alpha C}$ mutants, we noticed that BRAF$^{\Delta NVTAP}$, BRAF$^{\Delta LNVTAP>F}$, and BRAF$^{\Delta LNVTAP>Y}$ only differ in the amino acid residue at position 485 (fig. S1), with BRAF$^{\Delta LNVTAP>F}$ resembling the previously described point mutation L485F (*41*). Notably, while representing a smaller net deletion, BRAF^{delinsFS} also substitutes L485 by a phenylalanine residue, and the tyrosine introduced into BRAF$^{\Delta LNVTAP>Y}$ might entertain similar hydrophobic

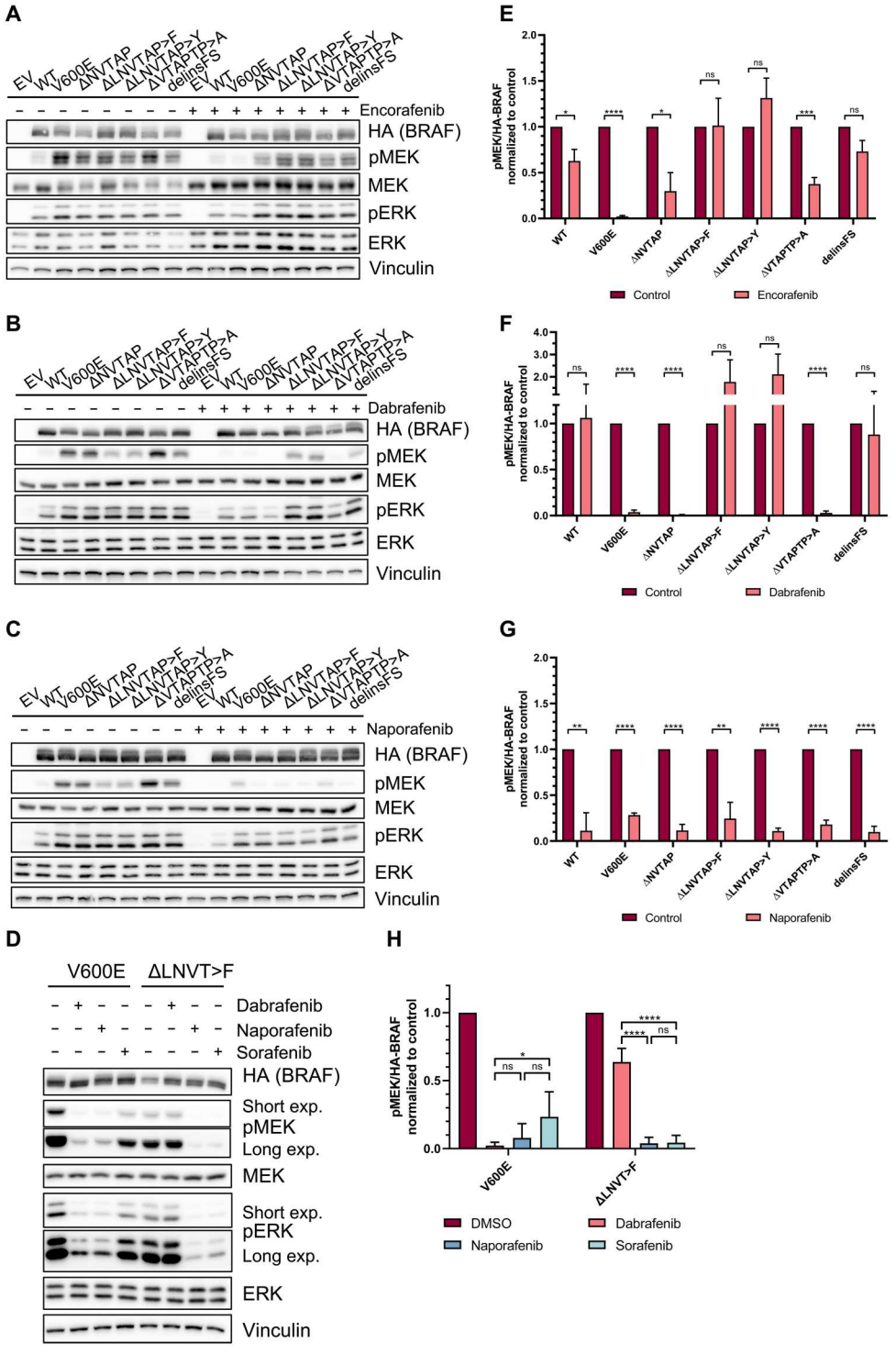
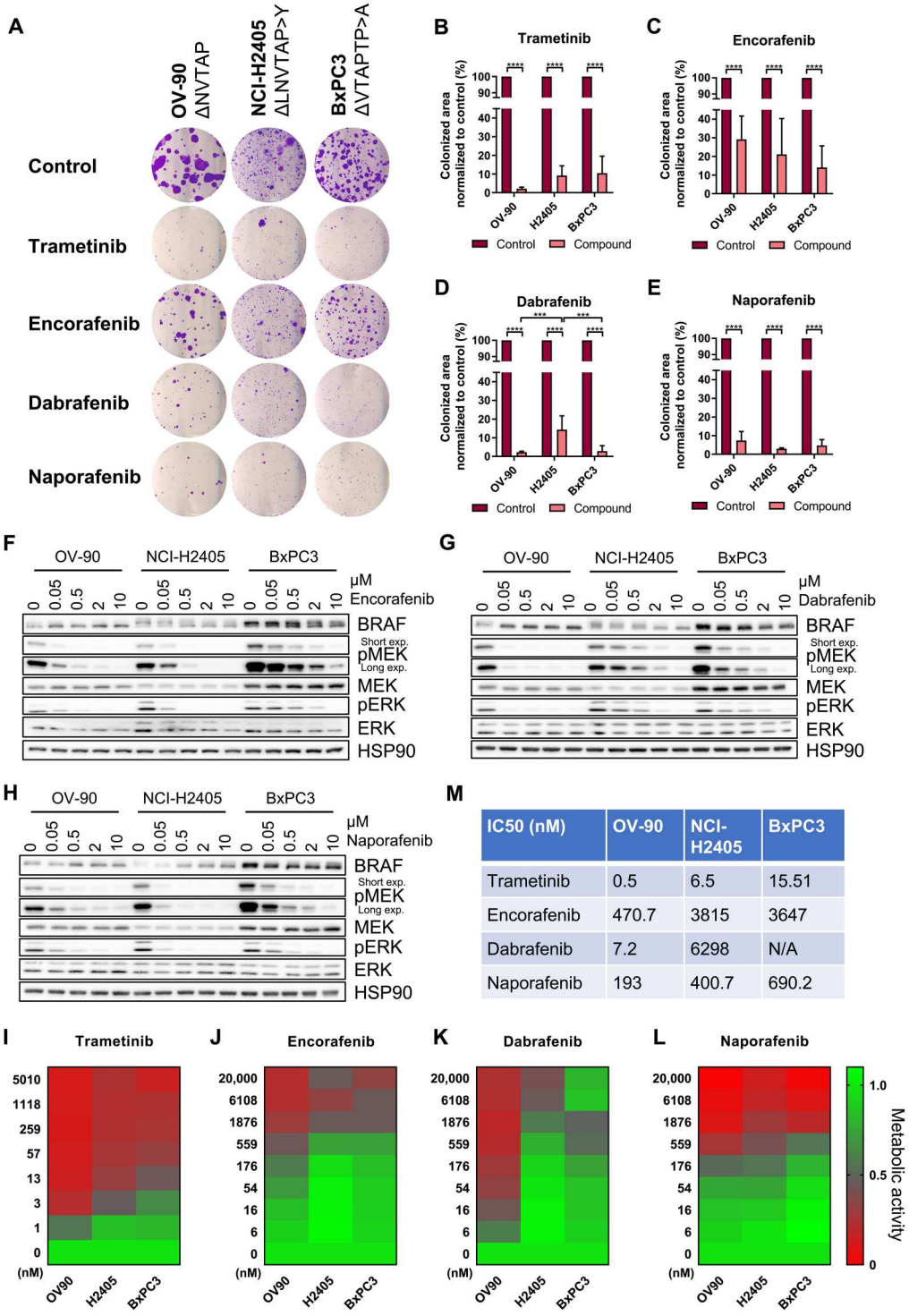


Fig. 5. BRAF$^{\Delta\beta3\text{-}\alpha C}$ mutants exhibit varying sensitivity to encorafenib and dabrafenib, but all of them are potently inhibited by dimer-targeting naporafenib. (**A** to **D**) The indicated HA-BRAF proteins were transiently expressed in HEK293T cells. Before lysis, cells were treated with encorafenib (0.5 μM), dabrafenib (1 μM), naporafenib (1 μM), sorafenib (10 μM), or vehicle control (DMSO) for 4 hours. The lysates were analyzed by immunoblot using the indicated antibodies. (**E** to **H**) Immunoblots were quantified using ImageJ. Bar graphs show calculated fold changes (inhibitor/control) of phospho-MEK levels normalized to HA-BRAF. The indicated inhibitors were compared to vehicle control (E) to (G) or each other (H) for each BRAF protein. BRAF^{V600E} served as a control. Statistical analysis: means + SD, $n = 3$, unpaired t tests with Holm-Šídák correction for multiple comparisons (E) to (G) or two-way ANOVA with Tukey's test for multiple comparisons (H), $^{*}P \leq 0.05$, $^{**}P \leq 0.01$, $^{***}P \leq 0.001$, $^{****}P \leq 0.0001$. Quantified phospho-ERK levels are shown in fig. S9.

interactions. In BRAF^{L485F}, F485 has been implicated to interact with F498, thereby creating a critical hydrophobic network that contributes to increased kinase activity and resistance to type I$^{1/2}$ inhibitors, including dabrafenib (*41*, *66*). As suggested by structural models of BRAF$^{\Delta NVTAP}$ and BRAF$^{\Delta LNVTAP>F}$, this aromatic interaction could also be established in BRAF$^{\Delta\beta3\text{-}\alpha C}$ variants exhibiting an aromatic amino acid residue at position 485 (fig. S12A). Therefore, we tested whether replacing F498 by an alanine residue could abrogate the differences between BRAF$^{\Delta\beta3\text{-}\alpha C}$ mutants (fig. S12, B and C). Unexpectedly, the F498A substitution strongly reduced the activity of BRAF$^{\Delta NVTAP}$, although the proposed aromatic interaction of F498 cannot be established in this mutant as L485 remains preserved (fig. S12A). In addition, the moderate reduction of BRAF^{V600E} activity upon F498A introduction suggests a broader



IC50 (nM)	OV-90	NCI-H2405	BxPC3
Trametinib	0.5	6.5	15.51
Encorafenib	470.7	3815	3647
Dabrafenib	7.2	6298	N/A
Naporafenib	193	400.7	690.2

Fig. 6. Encorafenib, dabrafenib, and naporafenib block the growth of BRAF$^{\Delta\beta3\text{-}\alpha C}$ mutant–expressing cell lines with varying efficacy. (**A**) Cells were cultivated in the presence of trametinib (5 nM), encorafenib (0.5 μM), dabrafenib (1 μM), naporafenib (1 μM), or vehicle control (DMSO). OV-90, NCI-H2405, and BxPC3 cells were fixed and stained with crystal violet after 16, 21, or 18 days, respectively. (**B** to **E**) The colonized area was determined using ImageJ. Bar graphs show the colonized area of inhibitor-treated cells normalized to the area of those treated with vehicle control. Statistical analysis: means + SD, n = 3, two-way ANOVA with Tukey's test for multiple comparisons, *$P \leq 0.05$, **$P \leq 0.01$, ***$P \leq 0.001$, ****$P \leq 0.0001$. (**F** to **H**) Western blot analysis showing the effect of the applied RAFis on MEK/ERK phosphorylation in the three cell lines. Detection of HSP90 serves as loading control. The corresponding quantification of pMEK levels is shown in fig. S15 (A to C). (**I** to **L**) Heatmaps showing the antiproliferative effect of trametinib, encorafenib, dabrafenib, and naporafenib on BRAF$^{\Delta\beta3\text{-}\alpha C}$ mutant–expressing cancer cell lines. Following incubation with inhibitor or vehicle control for 96 hours at the indicated concentrations, the metabolic activity was measured by XTT assay and normalized to vehicle control (n = 3). (**M**) Antiproliferation IC$_{50}$ values were calculated by nonlinear fitting using GraphPad Prism 9. Calculated fitted curves are shown in fig. S15 (D to G).

and hitherto unrecognized role of F498 in BRAF activity extending beyond the previously proposed interaction with L485F. In contrast to $BRAF^{\Delta NVTAP}$, pMEK levels of $BRAF^{\Delta LNVTAP>F}$ and $BRAF^{delinsFS}$ were only mildly reduced, suggesting that the de novo–inserted aromatic amino acid residue of $BRAF^{\Delta LNVTAP>F}$ or $BRAF^{delinsFS}$ could compensate for the loss of F498. In agreement with the model postulating an aromatic F485-F498 interaction (*41*, *66*), the F498A substitution reduced the intrinsic dabrafenib resistance of $BRAF^{\Delta LNVTAP>F}$, albeit by only 50% (fig. S12, D and E). While our manuscript was in initial review, we identified a previously unidentified exon 12 in-frame deletion mutant, $BRAF^{\Delta LNVT>F}$, in a melanoma case. This mutant provides an independent conformation for our hypothesis that aromatic amino acid residue substitutions of L485 play a central role in rendering $BRAF^{\Delta\beta3\text{-}\alpha C}$ mutants resistant to type $I^{1/2}$ inhibitors. $BRAF^{\Delta LNVT>F}$ differs from the previously characterized type$^{1/2}$ inhibitor–resistant mutants by its shorter net deletion of three amino acids (fig. S1). However, L485 was also substituted with a phenylalanine residue. As predicted from our analyses on $BRAF^{\Delta\beta3\text{-}\alpha C}$ variants with aromatic de novo amino acid insertions at position 485, $BRAF^{\Delta LNVT>F}$ was insensitive to dabrafenib. In contrast, naporafenib and sorafenib efficiently blocked the signaling output of $BRAF^{\Delta LNVT>F}$ (Fig. 5, D and H). In summary, all four $BRAF^{\Delta\beta3\text{-}\alpha C}$ variants with aromatic de novo amino acid insertions show intrinsic dabrafenib resistance.

Naporafenib blocks the proliferation of human cell lines expressing endogenous $BRAF^{\Delta\beta3\text{-}\alpha C}$ oncoproteins

The well-defined heterologous HEK293T system provides a strong advantage when comparing BRAF oncoproteins for their signaling output and druggability as it allows the comparison of the various mutants in question without the interference by cell line–specific comutations—a problem that might arise when comparing multiple cell lines. A disadvantage of this approach, however, is the ectopic overexpression of the oncoprotein in question outside of its histological context. This is particularly important as the histological context, which is mainly defined by the ontogeny of the cancer cell and its tumor microenvironment, is responsible for the contrasting drug responsiveness of various $BRAF^{V600E}$-driven tumor entities (*67*, *68*). Therefore, we assayed the drug responsiveness of three cell lines derived from ovarian (OV-90), non–small cell lung (NCI-H2405), and pancreatic (BxPC3) carcinoma that harbored three distinct endogenous $BRAF^{\Delta\beta3\text{-}\alpha C}$ oncoproteins, as we confirmed ourselves (fig. S13, A to C). Again, naporafenib and, as expected from its action downstream of $BRAF^{\Delta\beta3\text{-}\alpha C}$ oncoproteins, trametinib suppressed colony growth in all cell lines by more than 90% (Fig. 6, A to L). In contrast, encorafenib was less effective in all three cell lines, while the effects of dabrafenib on colony growth differed between the cell lines with the $BRAF^{\Delta NVTAP}$-expressing cell line OV-90 being the most sensitive. The high BRAF dependency of OV-90 is also reflected by the DepMap tool (https://depmap.org/portal/) that lists *BRAF* within the top 10 most essential genes for this but not the other two cell lines. Western blotting confirmed the successful but variable inhibition of the MEK/ERK pathway in all three cell lines, with the OV-90 cell line again responding best to encorafenib and dabrafenib (Fig. 6, F to H, and fig. S14, A to C). BxPC3 displayed the highest BRAF levels of these three cell lines, which agrees with the reported tetrasomy of the *BRAF*-containing chromosome 7 (*69*). As type $I^{1/2}$ inhibitor efficacy is modulated by the expression level of *BRAF* (*70*) and the ratio between its WT and mutant versions differing in drug affinity (*63*, *64*), it should be also kept in mind that NCI-H2405 lacks a $BRAF^{WT}$ allele, while OV90 and BxPC3 contain $BRAF^{WT}$ and $BRAF^{\Delta\beta3\text{-}\alpha C}$ alleles (fig. S13, A to C).

As naporafenib is still awaiting clinical approval, we asked whether sorafenib, a clinically extensively used type II inhibitor that has been crystalized with $BRAF^{\Delta NVTAP}$ (*36*), would yield similar effects (fig. S13, D and E). Four and ten micromolar sorafenib significantly reduced colony growth in all cell lines with endogenous $BRAF^{\Delta\beta3\text{-}\alpha C}$ mutations, and even 1 μM led to a slight but significant reduction in colony growth in OV-90 and NCI-H2405 cells. As these sorafenib concentrations are widely used in the field (*28*, *71*, *72*) and because peak plasma concentrations of up to 20 μM range were reported (*73*, *74*), our data suggest that this clinically available type II inhibitor could be further explored for the treatment of tumors driven by $BRAF^{\Delta\beta3\text{-}\alpha C}$ oncoproteins.

Next, we performed metabolic 2,3-bis-(2-methoxy-4-nitro-5-sulfophenyl)-2*H*-tetrazolium-5-carboxanilid (XTT) assays to determine half-maximal inhibitory concentration (IC_{50}) values for the three RAFi and trametinib in the three human cell lines with endogenously expressed $BRAF^{\Delta\beta3\text{-}\alpha C}$ oncoproteins (Fig. 6, I to M, and fig. S14, D to I). Similar to the colony growth and Western blot assays, the calculated IC_{50} values and the heatmaps demonstrate the relatively uniform responses of all three human cell lines to trametinib and naporafenib, while those to the type $I^{1/2}$ inhibitors encorafenib and dabrafenib varied considerably. Unexpectedly, we observed paradoxical metabolic activity in the pancreatic adenocarcinoma cell line BxPC3 at high dabrafenib concentrations, which precluded us from determining an IC_{50} for this cell line. As this phenomenon was not observed in the other cell lines, we exclude an artifact caused by chemical interference between dabrafenib and XTT. In addition to trametinib and the various RAFi, the ERK inhibitor ulixertinib (*75*, *76*) was similarly effective at clinically achievable concentrations in all three cell lines (fig. S14I).

Moreover, because BxPC3 expresses the $BRAF^{\Delta VTAPTP>A}$ variant, which was as efficiently inhibited as $BRAF^{\Delta NVTAP}$ by both type $I^{1/2}$ inhibitors in the HEK293T system (Fig. 5), we expected that the antiproliferative effects on OV-90 and BxPC3 cells would be comparable. To further investigate why BxPC3 differed so drastically from OV-90, we analyzed the phosphorylation status of EGFR and AKT, as we suspected an up-regulation of metabolic processes by compensatory hyperactivation of these signaling elements, e.g., by relief from MEK/ERK-mediated negative feedbacks or crosstalk (*55*, *77*–*80*). These analyses revealed two interesting differences between the three cell lines (fig. S14J). First, OV-90 lacked the prominent expression and autophosphorylation of EGFR observed in NCI-H2405 and BxPC3 cells. Second, BxPC3 exhibited high levels of AKT phosphorylated at the activating mTORC2 phosphorylation site S473 (*81*), which was further augmented by dabrafenib or naporafenib. This up-regulation might reflect the negative crosstalk between the ERK and AKT pathways that has been described for various cell types, including BxPC3 cells (*80*, *82*). Thus, in addition to the aforementioned differences between the three $BRAF^{\Delta\beta3\text{-}\alpha C}$ oncoproteins in terms of their RAFi sensitivity, differences in EGFR expression/activity and/or AKT activity could explain the increased sensitivity of OV-90 cells to the three RAFi and trametinib. Conversely, the unexpected mild-to-moderate effects of type $I^{1/2}$ inhibitors on BxPC3 cells could be due to the high activity of the PI3K/AKT signaling axis and the relief of

EGFR from negative feedback (*78*, *79*). Nevertheless, how naporafenib achieves substantial inhibition across the three cell lines (Fig. 6L), despite promoting phospho-AKT levels as well, requires further study. Collectively, these data, and, in particular, the phenotype of BxPC3 cells, demonstrate that the comparison of human cell lines with similar alterations in the pathway of interest is confounded by alterations such as co-mutations or chromosomal aberrations specific to each cell line and potentially cell-of-origin–related differences in gene expression.

Given the efficacy of the type II compounds naporafenib and sorafenib across all BRAF$^{\Delta\beta3\text{-}\alpha C}$ oncoproteins (Figs. 5 and 6 and fig. S8D), we combined them with the MEKi trametinib, which further increased the efficacy of these RAFi at nanomolar concentrations (Fig. 7, A to F). Notably, the sorafenib/trametinib combination has already been applied in the context of BRAF class III mutations (*83*) and advanced hepatocellular carcinoma (*84*), while first clinical data on naporafenib/trametinib combinations have recently been published for NRAS-driven melanoma (*85*). We also tested whether the efficacy of naporafenib could be further improved by the HSP90i XL888, which shows clinical activity in combination with vemurafenib in melanoma (*49*, *86*). In all three cell lines, however, XL888 exhibited a narrow range between not being additive to naporafenib and too toxic by itself to discern additive/synergistic effects with this RAFi (fig. S14, K to M). In summary, our analyses support the concept that the responsiveness of human cell lines expressing BRAF$^{\Delta\beta3\text{-}\alpha C}$ oncoproteins toward dabrafenib and encorafenib is modulated by the details of the BRAF in-frame deletion and their cellular context. In contrast, type II inhibitors, the MEKi trametinib, and the ERKi ulixertinib all impair viability in a uniform manner. Moreover, because sorafenib and trametinib were approved more than 10 years ago and because naporafenib is currently in clinical phase 2 trials, our data highlight potential clinically realizable vertical combination therapies for BRAF$^{\Delta\beta3\text{-}\alpha C}$-driven tumors.

Confirmation of type II RAFi efficacy in patient-derived organoids

As the three cell lines investigated have been established more than two decades ago, we next screened patient-derived organoids (PDOs) or associated unpublished datasets available to us for *BRAF* exon 12 in-frame deletions. We identified two PDAC PDOs harboring *BRAF*$^{\Delta NVTAP}$ mutations and investigated their drug responsiveness. The first dataset was derived from the COMPASS-0196 (NCT-04469556) PDO that was already drug tested before we identified the efficacy of naporafenib on BRAF$^{\Delta\beta3\text{-}\alpha C}$ mutants. In this PDO, the type II RAFi LY3009120, the two MEKi binimetinib and trametinib, and the ERKi SCH772984 were highly effective in suppressing PDO growth, while dabrafenib and encorafenib were only effective at very high concentrations (Fig. 8A). The underlying molecular mechanism remains unclear at present, but the presence of an ERBB3^{G507R} mutation, which is uncharacterized so far but is located in subdomain IV involved in dimerization control of this receptor tyrosine kinase (RTK), and a slight copy number variation (CNV) gain in *KRAS* (four copies) might have contributed to the paradoxical action of dabrafenib.

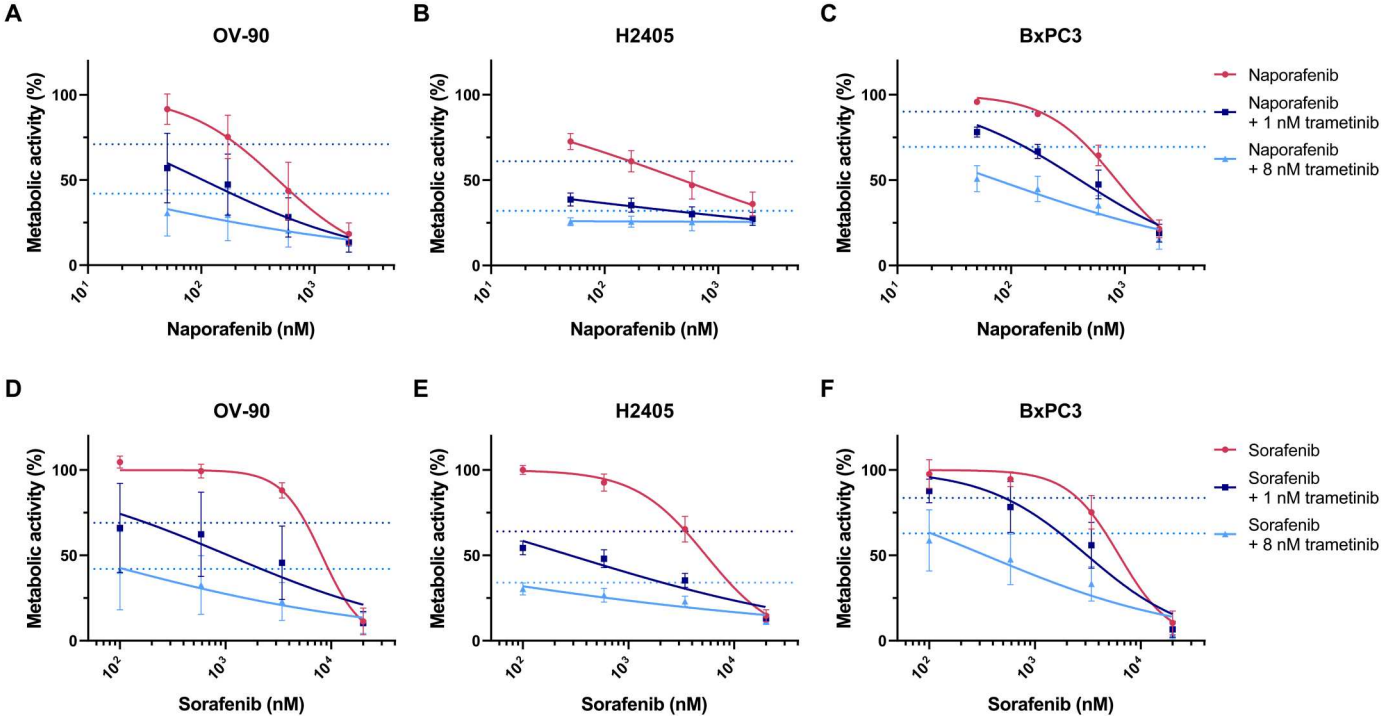


Fig. 7. Trametinib enhances the efficacy of type II RAFi. BRAF$^{\Delta\beta3\text{-}\alpha C}$ mutant–expressing cancer cell lines were incubated with naporafenib (**A** to **C**) or sorafenib (**D** to **F**) at the indicated concentrations, alone or combined with 1 or 8 nM trametinib, to explore the potential of vertical pathway inhibition. After 96 hours, the metabolic activity was measured by XTT assay and normalized to vehicle control. The metabolic activity in the absence of RAFis is indicated by dotted lines in the color of the respective trametinib concentration (dark blue, 1 nM trametinib; light blue, 8 nM trametinib). Graphs show the means + SD of three independent experiments. Nonlinear fitted curves were calculated using GraphPad Prism 9.

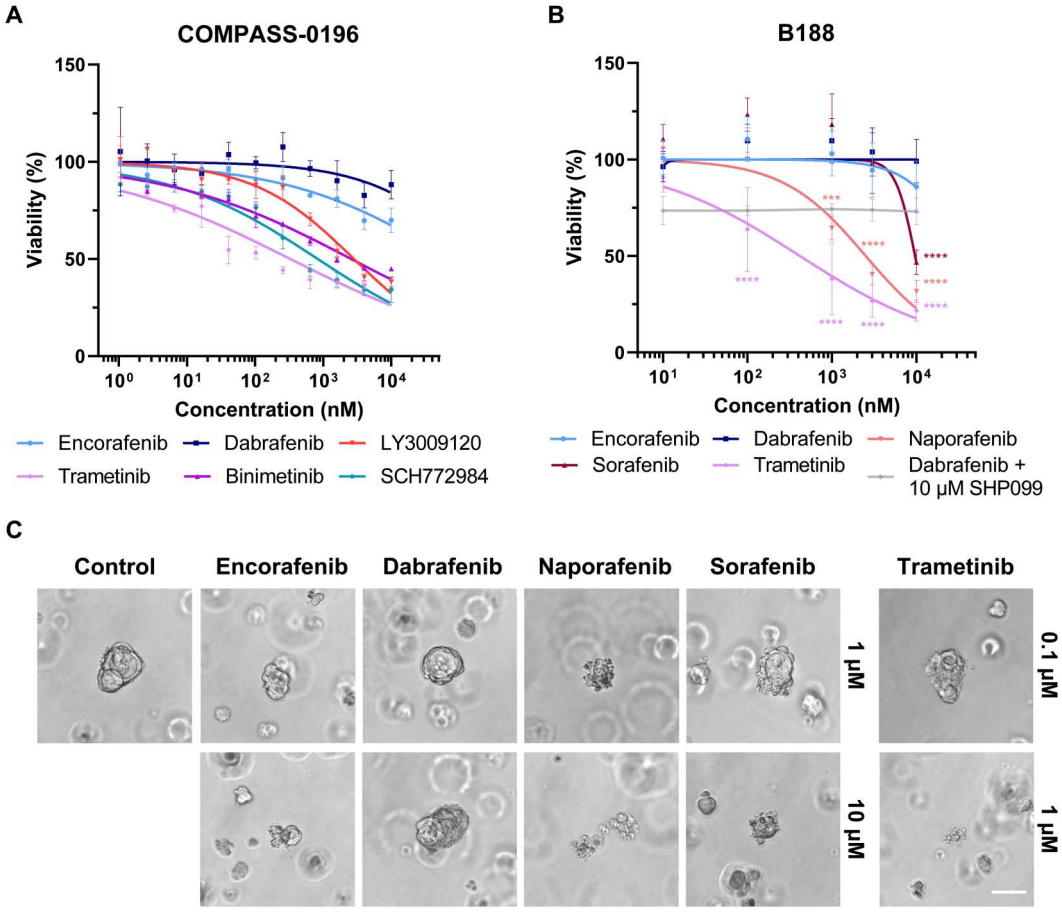


Fig. 8. Type II RAFi like naporafenib suppresses the growth and viability of PDAC PDOs. (**A**) COMPASS-0196 PDOs were treated with the indicated kinase inhibitors for 7 days. The viability was determined by CellTiter-Glo 3D assay and normalized to vehicle control. The graph shows the means + SD and calculated fitted curves of three independent experiments. (**B**) The viability of B188 organoids grown in the presence of the indicated inhibitors for 72 hours was determined using the CellTiter-Glo 3D assay and normalized to vehicle control (DMSO). Nonlinear fitted curves were calculated using GraphPad Prism 9. Statistical analysis: means + SD, $n = 4$ (dabrafenib + SHP099: $n = 3$), two-way ANOVA with Dunnett's test for multiple comparisons, $^{*}P \leq 0.05$, $^{**}P \leq 0.01$, $^{***}P \leq 0.001$, $^{****}P \leq 0.0001$. (**C**) Representative micrographs of inhibitor-treated B188 organoids right before performing the viability measurements shown in (B). Scale bar, 50 µM.

Given the aforementioned failure of LY3009120 in clinical trials and the data shown in Figs. 5 and 6, we generated another dataset of the B188 PDO using the type II RAFi naporafenib and sorafenib, the type $I^{1/2}$ compounds dabrafenib and encorafenib, as well as the MEKi trametinib. Trametinib and also both type II RAFi potently suppressed the viability of the PDO at clinically achievable concentrations (Fig. 8, B and C). Similar to the COMPASS-0196 PDO, dabrafenib and also encorafenib only showed slight effects at very high concentrations. As this finding is in contrast to the dabrafenib sensitivity of $BRAF^{\Delta NVTAP}$ mutant OV-90 cells, we screened the next generation sequencing (NGS) data of the B188 PDO for potential resistance mechanisms. Notably, we identified a previously unidentified E138Q mutation in GNA13 (fig. S13C). Although this mutation represents a variant of unknown significance, RAS/ERK activation has been observed in cells overexpressing this heterotrimeric G protein subunit (*87*, *88*). Consequently, one could envisage a paradoxical action of type $I^{1/2}$ inhibitors. Alternatively, but not excluding these possibilities, it is possible that, in contrast to the simple OV-90 culture medium, the organoid media enriched with EGF and fibroblast growth factor 10 (FGF10) could have contributed to paradoxical action of the type $I^{1/2}$ compounds and therefore could have blunted drug responses in both PDO models. In that regard, we combined dabrafenib with an allosteric SHP2 inhibitor to lower physiological RAS signaling (Fig. 8B). Although this compound by itself lowered viability by 25%, we did not observe significant additive effects with dabrafenib. Thus, identifying these confounding factors of dabrafenib resistance represents a project beyond the current study. Nevertheless, our cell line and PDO data already show that the *BRAF* exon 12 genotype represents only one criterion for inhibitor choice. Even if a dabrafenib-sensitive mutant is encountered, the spectrum of co-mutations and/or the ground state of the signaling network, e.g., RTK expression levels, might critically modulate dabrafenib responses. This insight represents a strong encouragement for more comprehensive genomic profiling before therapy. Moreover, a switch to type II inhibitors should be considered if primary or secondary drug resistance phenomena are encountered during dabrafenib therapy (fig. S16).

DISCUSSION

As comprehensive mutational screening of the entire *BRAF* coding sequence becomes diagnostic routine, more alterations outside of the classical hotspot exons 11 and 15 are discussed in MTBs. We noticed an increase in enquiries and literature concerning *BRAF* exon 12 alterations, most notably Δβ3-αC in-frame deletions (*31*, *32*, *34*, *39*, *89*). For example, 3.15% of *KRAS* WT PDACs analyzed in a multicenter study carried such alterations (*90*). Depending on the cohort, Chen *et al.* (*35*) reported a prevalence between 2.3 and 7.1% in *KRAS* WT pancreatic carcinoma. Considering the 458,918 new cases of pancreatic carcinoma reported in 2018 (*91*) and that ~5 to 10% of these lack *KRAS* alterations, we estimate that several thousand patients of this disease group alone will be potentially diagnosed with druggable $BRAF^{\Delta\beta3\text{-}\alpha C}$ mutants annually. We expect that more exon 12 variants will be found in the future, and here, we extend their spectrum by identifying and characterizing two previously unidentified mutants, $BRAF^{delinsFS}$ and $BRAF^{\Delta LNVT>F}$. The $BRAF^{\Delta\beta3\text{-}\alpha C}$ mutants originally identified within human neoplasms have been recently observed in 19% of canine urothelial carcinoma (*92*), highlighting the possibility that studying their pathobiology and druggability will bridge between human and veterinarian oncology.

From our experience, two major questions are recurrently raised in MTBs regarding $BRAF^{\Delta\beta3\text{-}\alpha C}$ mutants. The first concerns their general relevance as oncogenic drivers, in particular, as activity correlates with deletion length (*36*, *37*). So far, all $BRAF^{\Delta\beta3\text{-}\alpha C}$ mutants turned out to be very potent oncogenic drivers and $BRAF^{delinsFS}$ and $BRAF^{\Delta LNVT>F}$, despite their shorter deletion, are no exception. On the basis of our functional analyses (Fig. 2, A and B) and previous studies (*35*, *66*), we posit that all $BRAF^{\Delta\beta3\text{-}\alpha C}$ oncoproteins owe their high signaling potential to their high dimerization propensity that stems from their αC helices locked in the IN position. In that regard, $BRAF^{\Delta\beta3\text{-}\alpha C}$ oncoproteins imitate a conformation into which WT RAF proteins are transferred during dimerization. Recent structural modeling proposes that dimerization breaks protomer-internal hydrophobic interactions mediated by so-called π-π stacking and replaces them with intermolecular π-π bonds formed between aromatic amino acid residues in both protomers (*15*). These interactions reorientate the αC helix and the HRD motif, leading to kinase activation through R-spine formation (*41*, *93*). Consequently, the high dimerization propensity of $BRAF^{\Delta\beta3\text{-}\alpha C}$ oncoproteins promotes full kinase activation and MEK phosphorylation, which is facilitated by dimeric RAF (*24*).

The second and even more pressing question is which targeted therapy compounds are the most appropriate for treating tumors carrying *BRAF* exon 12 in-frame deletions. Given the high activity of $BRAF^{\Delta\beta3\text{-}\alpha C}$ mutants, tumors driven by these oncoproteins qualify for a treatment regimen involving MEKi, as also reflected by therapeutic responses of several PDAC cases (*31*, *34*) and a Langerhans cell histiocytosis (LCH) (*94*). In $BRAF^{V600E}$-driven tumors, however, MEKi are usually combined with $BRAF^{V600E}$-selective drugs to achieve more sustainable therapeutic outcomes (*95*). On the basis of pathway topology, it can be expected that this concept is also applicable to other cancers driven by highly active non-V600E BRAF mutants. Moreover, the emerging concept of low-dose vertical pathway inhibition (*51*, *96*) highlights the necessity to identify compounds effectively and directly inhibiting $BRAF^{\Delta\beta3\text{-}\alpha C}$ oncoproteins for future treatment regimen. Here, we show that oncogenic signaling by all $BRAF^{\Delta\beta3\text{-}\alpha C}$ mutants we investigated can be efficiently inhibited by the type II RAFi naporafenib and sorafenib. As these drugs are in clinical trials and use, respectively, our data might inform decisions concerning the inclusion of patients into clinical trials involving naporafenib and other emerging third-generation RAFis, or to recommend off-label and compassionate use of sorafenib. As suggested previously (*35*, *36*) and as extended by fig. S8D, other type II inhibitors in (pre)clinical development might represent attractive alternatives as well.

The varying efficacy of the type $I^{1/2}$ inhibitors vemurafenib, dabrafenib, and encorafenib against $BRAF^{\Delta\beta3\text{-}\alpha C}$ mutants represents an interesting aspect from both a clinical and a basic kinase biochemistry perspective. We confirm previous observations that vemurafenib is ineffective against $BRAF^{\Delta\beta3\text{-}\alpha C}$ mutants (*35*, *36*), while encorafenib, an inhibitor not yet tested on these oncoproteins, shows limited and probably insufficient activity. In line with case reports demonstrating therapeutic responses of two $BRAF^{\Delta NVTAP}$-positive PDACs (*89*, *97*) and an LCH (*98*) to (initial) dabrafenib monotherapy, we [and (*35*)] show that dabrafenib strongly suppresses $BRAF^{\Delta NVTAP}$-driven MEK/ERK phosphorylation in OV-90 cells. While our manuscript was under review, another case report presented an at least 18-month-lasting partial response of a melanoma containing a similar $BRAF^{\Delta NVTAP}$ mutant to dabrafenib/trametinib combination therapy (*99*). As there is now more than a decade of clinical experience with dabrafenib, the efficacy of this compound against $BRAF^{\Delta\beta3\text{-}\alpha C}$ oncoproteins is of particular interest. Chen *et al.* (*35*), however, observed that dabrafenib only had minimal effects on MEK/ERK phosphorylation in NCI-H2405 ($BRAF^{\Delta LNVTAP>Y}$) and BxPC3 ($BRAF^{\Delta VTAPTP>A}$) cells. We reproduced these findings (Fig. 6G) and decided to use our heterologous HEK293T model, which does not harbor the caveat of distinct genetic and histological backgrounds, as it is the case for cell lines, to clarify whether the difference in dabrafenib sensitivity is linked to the individual deletion type. Only $BRAF^{\Delta NVTAP}$ and $BRAF^{\Delta VTAPTP>A}$ displayed dabrafenib sensitivity (Fig. 5F). As $BRAF^{\Delta LNVTAP>F}$ showed a significantly higher propensity for homodimerization than $BRAF^{\Delta NVTAP}$ (Fig. 3, A and B), it is tempting to attribute the observed dabrafenib resistance of the former to increased dimerization and negative allostery (*19*). In that regard, Foster *et al.* (*36*) demonstrated that, in contrast to dabrafenib, vemurafenib induces and requires a greater αC helix shift during inhibitor accommodation that cannot be provided by $BRAF^{\Delta NVTAP}$ because of the sterical constraints imposed by the in-frame deletion. Therefore, the dabrafenib-resistant $BRAF^{\Delta LNVTAP>F}$, $BRAF^{\Delta LNVTAP>Y}$, $BRAF^{\Delta LNVT>F}$, and $BRAF^{delinsFS}$ mutants (Fig. 5, B, F, D, and H), which have not yet been investigated for their impact on αC helix flexibility, might differ from $BRAF^{\Delta NVTAP}$ in such a way that their deletions, which are accompanied by insertions of a bulky aromatic residue, preclude dabrafenib binding by negative allostery. The aforementioned study by Zhang *et al.* (*15*), who describe the critical role of hydrophobic interactions occurring during RAF activation, proposes that dimerization tightens the adenosine triphosphate–binding pocket and thereby interferes with inhibitor accommodation by steric clashes in which minute differences between the various RAFi might have large effects.

Another recent study, however, showed that the binding affinities of the dimer-favoring type II inhibitor naporafenib and dabrafenib to chemically enforced $BRAF^{V600E}$ dimers are comparable, demonstrating that increased dimerization is insufficient to confer

resistance to type $I^{1/2}$ inhibitors (*25*). Moreover, the inability of the R509H substitution, alone or combined with the AAE mutation, to improve dabrafenib sensitivity in $BRAF^{\Delta LNVTAP>F}$ suggests that other mechanisms decide drug accommodation (fig. S11). For example, the mechanism for dabrafenib resistance could be explained by the hydrophobic network that underlies the formation of the R-spine (*15*, *41*). In that respect, we noted that $BRAF^{\Delta LNVTAP>F}$, $BRAF^{\Delta LNVTAP>Y}$, $BRAF^{\Delta LNVT>F}$, and $BRAF^{delinsFS}$ substitute L485 for a bulky aromatic residue that could restrict dabrafenib binding, while the in terms of deletion length similar $BRAF^{\Delta VTAPTP>A}$ mutant remained dabrafenib sensitive. This concept is supported by a study proposing that the introduced phenylalanine of the $BRAF^{L485F}$ point mutant forms a hydrophobic network with F498, which in turn stabilizes the R-spine and precludes type $I^{1/2}$ inhibitor binding (*66*). Consequently, loss of F498 should break dabrafenib resistance. The F498A substitution reduced the dabrafenib resistance of $BRAF^{\Delta LNVTAP>F}$ by 50% (fig. S12, D and E). This finding supports this model but also suggests that other mechanisms contribute to the dabrafenib resistance of $BRAF^{\Delta LNVTAP>F}$, $BRAF^{\Delta LNVTAP>Y}$, $BRAF^{\Delta LNVT>F}$, and $BRAF^{delinsFS}$. Therefore, the insertion of de novo hydrophobic amino acids at the in-frame deletion junction might generate a distinct mutation-specific hydrophobic network or modify the already recognized ones (*15*) and thereby increase dimerization propensity, activity, and type $I^{1/2}$ RAFi resistance. This represents an interesting area for future studies. Moreover, as the spectrum of tumor-associated $BRAF^{\Delta\beta3\text{-}\alpha C}$ will probably expand in the near future, we will learn whether there is a selective pressure for maintaining or even replacing L485 with bulky hydrophobic residues to increase oncogenic potential and type $I^{1/2}$ inhibitor resistance. By revisiting the deletion walking experiment by Foster and colleagues (*36*), we realized that their data also support the critical role of L485 as in-frame deletions omitting L485 hardly increased the MEK phosphorylation potential of BRAF. The analysis of $BRAF^{\Delta LNVTAP>F}$ crystal structures, which are not available to date, could potentially reveal the mechanisms conferring resistance against type $I^{1/2}$ RAFis. Close inspection of the orientation and potential intramolecular interactions of F485 of $BRAF^{\Delta LNVTAP>F}$ compared to those of L485 of $BRAF^{\Delta NVTAP}$ will be key. Although the precise mechanism(s) of dabrafenib resistance need to be addressed in separate studies, our data already demonstrate that $BRAF^{\Delta\beta3\text{-}\alpha C}$ oncoproteins significantly differ in their sensitivity toward this compound. Thus, extra caution must be applied when experiences from individual case reports with marked responses for one $BRAF^{\Delta\beta3\text{-}\alpha C}$ mutant to dabrafenib are used as evidence to tailor a therapy for an oncoprotein with a seemingly highly similar but distinct alteration.

We also obtained previously unknown insights into the requirements of $BRAF^{\Delta\beta3\text{-}\alpha C}$ mutants for oncogenic signaling. A major open question was whether $BRAF^{\Delta\beta3\text{-}\alpha C}$ mutants signal as monomers or (constitutive) dimers (*24*, *35*–*37*). In hindsight, this controversy was partly caused by the fact that the various laboratories investigated distinct $BRAF^{\Delta\beta3\text{-}\alpha C}$ mutants and used the R509H mutation as a tool to measure dimer dependency. In that regard, the R509H mutation reliably blocks allosteric transactivation, a process from which $BRAF^{V600E}$ and potentially other high-activity mutants are largely exempted (*9*). However, while the R509H mutation strongly reduces homodimer affinity, it does not completely abrogate dimerization, and only the additional introduction of the AAE mutation really renders almost all BRAF molecules monomeric, at least according to coimmunoprecipitation experiments. Thus, the suitability of the R509H mutation to discriminate between dimeric and monomeric BRAF needs to be taken with caution, in particular, within the context of mutants with high dimerization propensity (*24*). Therefore, we revisited the dimerization potential of $BRAF^{\Delta\beta3\text{-}\alpha C}$ mutants and demonstrate that they form very stable homodimers with a significantly higher efficiency than $BRAF^{V600E}$. On the basis of these data and work by others on $BRAF^{\Delta NVTAP}$ and other in-frame deletion mutants (*24*, *35*), we conclude that $BRAF^{\Delta\beta3\text{-}\alpha C}$ mutants signal as dimers because they lose their high MEK phosphorylation and dimerization potential upon the simultaneous introduction of the R509H and AAE mutations. We interpret the relative resistance of the $BRAF^{\Delta\beta3\text{-}\alpha C}$ mutants toward the R509H mutation by the aforementioned structural peculiarities of these oncoproteins that, due to their special αC helix conformation, lock them in an active state. Thereby, they become independent of allosteric transactivation that is critical for other BRAF gain-of-function mutants (*3*). Like $BRAF^{V600E}$, but unlike other BRAF oncoproteins (*18*, *40*), Δβ3-αC mutants signal independent of $D^{594}FGLATV^{600}KS$-motif phosphorylation, which further supports the notion that the in-frame deletion constitutively induces the active αC-helix-IN/DFG-IN/R506-IN conformation. In all these respects, $BRAF^{\Delta\beta3\text{-}\alpha C}$ mutants resemble the canonical class I mutant $BRAF^{V600E}$, although their varying sensitivity toward type $I^{1/2}$ inhibitors argues against this categorization. Thus, these oncoproteins might constitute a class of their own. Another notable parallel to $BRAF^{V600E}$ is the ability of $BRAF^{\Delta\beta3\text{-}\alpha C}$ mutants to form large multiprotein complexes. We demonstrated previously that these large multiprotein complexes reflect BRAF activity as endogenous $BRAF^{V600E}$ shifts to the small complex upon vemurafenib treatment (*23*). As we had demonstrated that the large $BRAF^{V600E}$-containing complex is enriched with the HSP90/CDC37 complex and because $BRAF^{V600E}$ shows a specific vulnerability toward HSP90 inhibition (*47*, *48*, *86*), we investigated the association of $BRAF^{\Delta\beta3\text{-}\alpha C}$ mutants with HSP90. $BRAF^{delinsFS}$ recruits HSP90 to a similar extent as $BRAF^{V600E}$, while recruitment of HSP90 to $BRAF^{\Delta NVTAP}$ was even more pronounced. Unexpectedly, $BRAF^{\Delta LNVTAP>F}$ recruits less of this chaperone. In line with this result, $BRAF^{\Delta NVTAP}$ and $BRAF^{V600E}$ become unstable in the presence of the clinically trialed HSP90 inhibitor XL888 and present with a significantly shorter half-life. Commensurate with its lower HSP90 recruitment propensity (like $BRAF^{WT}$), $BRAF^{\Delta LNVTAP>F}$ displays higher overall stability in our tet-washout experiments and in the presence of XL888. It is tempting to speculate that the very high homodimer formation shown by $BRAF^{\Delta LNVTAP>F}$ stabilizes this oncoprotein and alleviates the need for being chaperoned by HSP90/CDC37.

Two recent studies might provide additional explanations for the contrasting HSP90 binding behavior of $BRAF^{\Delta\beta3\text{-}\alpha C}$ mutants (*100*, *101*). Using cryo–electron microscopy (cryo-EM), it was shown that the HSP90/CDC37 complex binds to the C-lobe of the kinase domains of BRAF and RAF1, while the latter, which shows higher affinity to the chaperone complex, also binds to the N-lobe and in the vicinity of the Δβ3-αC segment (*101*). This interaction requires the unfolding of the N-lobe, which remains folded in the context of $BRAF^{WT}$ but becomes unstructured and more RAF1-like in the context of the specific conformation of $BRAF^{V600E}$ imposed by the aforementioned salt bridge linking N- and C-lobes. This explains why $BRAF^{V600E}$ tightly interacts with this chaperone (*23*)

and is exquisitely sensitive to HSP90 inhibition (*47*, *48*). Thus, deletion of Δβ3-αC segment might restructure the BRAF N-lobe in such a way that it becomes an interaction point for the HSP90/CDC37 complex. This concept would explain why several but not all BRAF$^{\Delta\beta3\text{-}\alpha C}$ mutants tightly copurify with HSP90/CDC37 and how specific details of the in-frame deletion modulate this interaction. The BRAF$^{\Delta LNVTAP>F}$ mutant and, potentially due to structural similarities, BRAF$^{\Delta LNVTAP>Y}$ represent a notable exception for the increased HSP90 binding observed for other BRAF$^{\Delta\beta3\text{-}\alpha C}$ oncoproteins (Fig. 3, A, B, and D). On the basis of very recent insights from cryo-EM and deuterium exchange/MS experiments showing that the HSP90/CDC37 complex recognizes RAF molecules with N and C loop unfolded (*101*–*103*) and the notion that R-spine formation–induced conformational changes are a prerequisite for efficient N- and C-loop compaction and hence DIF-mediated dimerization (*15*, *17*, *93*), we posit that it is the high dimerization propensity of BRAF$^{\Delta LNVTAP>F}$ that precludes its interaction with the chaperone complex. This hypothesis is supported by our experiment in which the R509H and AAE mutations increased HSP90 binding of BRAF$^{\Delta LNVTAP>F}$ (Fig. 3D). Although this represents an area for future studies, our present data nevertheless suggest that inhibitors targeting specific HSP90/CDC37 complexes could be useful to treat tumors driven by other BRAF$^{\Delta\beta3\text{-}\alpha C}$ mutants, e.g., to enhance the efficacy of RAFi. Therefore, our study highlights the so-far unrecognized functional diversity of BRAF$^{\Delta\beta3\text{-}\alpha C}$ oncoproteins and recommends that precision and attention to molecular details must be applied when potentially effective but highly discriminating type I$^{1/2}$ inhibitors like dabrafenib are considered. Encouraging responses with dabrafenib were observed in individual PDAC cases of BRAF$^{\Delta NVTAP}$-driven tumors (*89*, *97*) and in the OV-90 cell line containing the same in-frame deletion (Fig. 6, A, D, G, M, and K). However, two BRAF$^{\Delta NVTAP}$-containing PDAC PDOs hardly responded to clinically meaningful dabrafenib concentrations, possibly because of private co-mutations as discussed above. Likewise, the BxPC3 cell line containing the dabrafenib-sensitive BRAF$^{\Delta VTAPTP>A}$ mutant appeared less BRAF addicted, probably because of its high pAKT levels. Thus, our data suggest an algorithm for targeted therapy recommendations (fig. S16) based on structural differences predicting intrinsic dabrafenib sensitivity/resistance and based on private comutations and/or expression levels of signaling elements modulating dabrafenib responsiveness. Last, our data provide impetus for the clinical development of safe and effective pan-RAFis that block the activity of all BRAF$^{\Delta\beta3\text{-}\alpha C}$ oncoproteins, irrespective of their intrinsic dabrafenib sensitivity or the private signaling network of the tumor cells.

MATERIALS AND METHODS

Patient

The patient had given written informed consent for molecular analysis (whole-genome/exome and RNA sequencing, DNA methylation profiling) within NCT/DKTK MASTER, a prospective observational and registry study approved by the Ethics Committee of Heidelberg University (protocol number S-206/ 2011) in which patients with advanced rare cancers and patients diagnosed with advanced common cancers at an unusually young age undergo a standardized precision oncology workflow, including clinical decision-making in a multi-institutional MTB (*38*, *104*).

Cell lines and genomic DNA analysis

Plat-E cells were provided by T. Kitamura (University of Tokyo). HEK293T cells were provided in-house by A. Hecht. Plat-E, HEK293T cells, and pBABE-puro-CreER^{T2}-transduced *Braf*$^{floxE12/floxE12}$ MEF, which were generated in-house and are immortalized by simian virus 40 large T antigen expression (*9*), were cultivated in Dulbecco's modified Eagle's medium (DMEM) (4.5 g/liter glucose) supplemented with 10% fetal calf serum (FCS), 2 mM L-glutamine, 10 mM Hepes, penicillin (200 U/ml), and streptomycin (200 μg/ml). OV-90 and NCI-H2405 cells were purchased from American Type Culture Collection. BxPC3 cells were a gift of S. Diederichs (University Medical Center Freiburg). These three cell lines were maintained in RPMI 1640 supplemented with 10% FCS, 2 mM L-glutamine, 10 mM Hepes, penicillin (200 U/ml), and streptomycin (200 μg/ml) and were authenticated by genomic DNA (gDNA)–based PCR analysis confirming the presence of the *BRAF* mutations previously reported for these cell lines (*35*, *36*). To this end, gDNA was extracted using standard protocols and used as template for a PCR using Phusion polymerase (NEB) and oligonucleotides matching to introns 11 (5′- GGAGGATCCCCATGGAACAAACAAGGTTG-3′) and 12 (5′-GGAGAATTCCCACCTCTAAATGTATTCTG-3′) of *BRAF*. PCR amplicons were subcloned into pSC-A (Stratagene) for further analysis (fig. S12, A to C). Absence of mycoplasma was confirmed by PCR (Eurofins Genomics, Ebersberg, Germany).

PDO establishment, culture, and drug tests

The COMP-196 PDO was identified within a cohort of PDAC PDOs established at the Princess Margaret Cancer Centre Living Biobank (https://pmlivingbiobank.uhnresearch.ca/) from patients enrolled in the COMPASS trial (*105*, *106*) and using procedures previously described in detail for xenograft-derived organoids (*107*). In brief, percutaneous core biopsy tissue from a liver metastasis was minced and dissociated in 1 ml of advanced DMEM (adDMEM)/F12 with 100 μl of Liberase TH (Sigma-Aldrich) and 10 μM Y-27632 at 37°C for 15 min. Cell pellets were washed with adDMEM/F12, counted, and plated in Matrigel with modified human organoid medium [adDMEM/F12, 20% (v/v) Wnt-3a conditioned media, 30% (v/v) R-Spondin1 conditioned media, 1× B27, 2 mM GlutaMAX, 10 mM Hepes, antibiotic-antimycotic (100 U/ml), 1 mM nicotinamide, 1.25 mM *N*-acetyl cysteine, 10 nM gastrin I, hNoggin (100 ng/ml), FGF10 (100 ng/ml), EGF (50 ng/ml), 0.5 μM A 83-01, 10 μM Y-27632, and 2.5 μM CHIR-99021]. For drug tests, domes were dissolved and passaged in TrypLE (Gibco) for 30 to 60 min and counted in trypan blue. Cells were seeded in 10 μl of Matrigel in a 384-well plate at 1000 cells per well overlain with 40 μl of human organoid media (day 1). After 24-hour recovery, drugs were added using a Tecan D300e dispenser (day 2). Viability was measured using Cell Titre Glo 3D after 1 week (day 8).

The B188 PDO was identified within a cohort of pancreatic carcinoma PDOs established at the University Medical Centre Freiburg, Germany. Informed consent was obtained from patients for the establishment and use of three-dimensional (3D) organoid cultures from human pancreatic cancer tissue samples. Sampling was approved by the local Ethics Committee of the University of Freiburg Medical Center (126/17; 28 March 2017). Surgery was performed at the Department of General and Visceral Surgery of the University Hospital Freiburg for proven or suspected pancreatic cancer. Organoid derivation and cultivation protocols were

adapted from previous publications (*108*, *109*). In brief, tissue samples were minced into small fragments and digested in 3 ml of complete collagenase digestion buffer [1× human complete feeding medium (COM), Collagenase Crude Type XI (5 mg/ ml; Sigma-Aldrich), 10.5 μM Y-27632, and deoxyribonuclease (DNAse) (10 μg/ml)]. COM consists of 1× HuWa medium [1× adDMEM/ F-12, 10 mM Hepes (pH 7.2 to 7.5), 1× GlutaMAX supplement (all three from Gibco), and Primocin (100 μg/ml; InVivoGen)], 1× Wnt3a-conditioned medium or Afamin/Wnt3a-conditioned medium, 1× R-Spondin1–conditioned medium, 1× B27 supplement (Gibco), 10 mM nicotinamide, 1.25 mM *N*-acetylcysteine (both from Sigma-Aldrich), Plasmocin (2.5 μg/ml; InVivoGen), hEGF (50 ng/ml), hFGF10 (100 ng/ml), 10 nM hGastrin I (all three from PeproTech), 500 nM A 83-01 (TOCRIS), and 10.5 μM Y-27632 (Sigma-Aldrich).

In total, two incubation steps in a rotating incubator were performed at 37°C for 15 min. After each incubation, the digested tissue was manually triturated 10 to 20 times, and the supernatant of both fractions was centrifuged at 4°C, 200*g* for 5 min. The cells were resuspended in 2 ml of ACK lysing buffer (Gibco), incubated for 2 min, and spun again. Subsequently, the cells were washed once with HuWa medium containing 0.1% bovine serum albumin (BSA; Sigma-Aldrich). The cell pellet was resuspended in an adequate amount of Matrigel (8 mg/ml; Corning). New domes with 25 μl of Matrigel each were made and incubated at 37°C, 5% CO_2 for 15 to 20 min. Thereafter, 500 μl of Complete Organoid Medium with Wnt (COM-Wnt) or Wnt-Afamin (COM-W/A) supplemented with 10.5 μM Y-27632 was added. PDOs were grown 6 to 12 days at 37°C, 5% CO_2 and checked every third day. NGS sequencing leading to the identification of the *BRAF*$^{\Delta NVTAP}$ mutation was performed at University Spital Zürich, Molecular Pathology department (sequencing type, FoundationOne CDx).

To passage PDOs, two Matrigel domes were pooled and dissolved in 500 μl of ice-cold cell recovery solution (CRS). Subsequently, the suspension was incubated for 30 min on ice, inverting the tube every 10 min. The cells were pelleted, and the CRS was discarded. The cell pellet was resuspended in 2 ml of TrypLE Master mix [1.5 ml of 1× TrypLE Express Enzyme (Gibco), 0.5 ml of HuWawith, 0.1% BSA, 10.5 μM Y-27632, and DNase (10 μg/ml)]. The cells were incubated in a rotating incubator at 37°C and 180 rpm for 15 min. Cells were pelleted again, and the supernatant was aspirated. The cell pellet was resuspended 20 times in ice-cold HuWa medium with 0.1% BSA to mechanically dissociate the PDOs. Following a last centrifugation step, cells were resuspended in Matrigel, and new domes (25 μl of Matrigel each) were spotted into tissue culture wells incubated at 37°C, 5% CO_2 for 15 to 20 min before being overlain with 500 μl of COM-Wnt or COM-W/A supplemented with 10.5 μM Y-27632. Occasionally, an aliquot of cells was used to isolate gDNA as described above to confirm the presence of driver mutations.

For drug tests, PDO-containing domes were dissolved as described above, and isolated cells were counted with a Bio-Rad TC20 Automated Cell Counter. Desired number of cells was seeded in a 96-well plate in 5 μl of Matrigel domes with 1000 cells per dome. After incubation at 37°C, 5% CO_2 for 15 min, 100 μl of COM-W/A medium was added per well. In addition, all empty wells were filled with 120 μl of phosphate-buffered saline (PBS) to decrease medium evaporation. Following cultivation (5% CO_2, 37°C) for 7 days, the medium was carefully aspirated, and the drugs diluted in either COM-W/A or HuWa were added and incubated for 3 days. Subsequently, 100 μl of Cell Titer Glo 3D (Promega) was added to the wells and resuspended 10 times. After incubation for 30 min in the dark at room temperature, the luminescence signal was measured with a Tecan infinite M200 plate reader (integration time, 100 ms).

Generation of pCLXEBR-pTF1-HA-BRAF-IRES-GFP (pCLXEBR) MEFs

To generate *Braf*$^{floxE12/floxE12}$ MEFs expressing HA-BRAF proteins upon Tet/Dox induction, recombination of *Braf*$^{floxE12/floxE12}$ MEFs was induced by treatment with 4-hydroxytamoxifen (1 μM). Efficient recombination was confirmed by genomic PCR (*110*) and Western blot analyses (fig. S15). *Braf*$^{-/-}$ MEFs were infected with ecotropic lentiviral particles using the packaging plasmids psPAX2 and pCMV_Eco provided by I. Frew (*111*). Successfully infected cells were selected with blasticidine S (5 μg/ml).

Plasmids

The generation of the bicistronic retroviral vectors pMIG and pMI-Berry encoding N-terminally HA-tagged or C-terminally Myc-tagged human BRAF, respectively, as well as the point mutants V600E and F595L was described previously (*9*, *44*). Δβ3-αC mutations, the F498A, and the dimerization-impairing mutations R509H and 621APE-AAE were introduced via site-directed mutagenesis using the oligonucleotides specified in table S1.

To generate tet-inducible pCLXEBR-pTF1-HA-BRAF-IRES-GFP constructs, the HA-BRAF-IRES-GFP insert was excised from corresponding pMIG constructs using *BsrG*I. The tet-inducible pCLXEBR-pTF1-kRasV12 vector, which we obtained from Addgene (plasmid no. 114318; deposited and provided by P. Salmon), was digested with *BsrG*I, thereby removing the kRasV12 encoding insert, followed by ligation of HA-BRAF-IRES-GFP insert and pCLXEBR-pTF1 vector backbone.

Antibodies and reagents

Antibodies used in this study were anti–B-RAF (D9T6S), anti-GFP, anti-HSP90, anti-p44/42 MAPK (ERK1/2), anti–phospho-p44/22 (ERK1/2) (Thr^{202}/Tyr^{204}), anti-MEK1/2, anti–phospho-MEK1/2 (Ser$^{217/212}$), anti-AKT, anti–phospho-AKT (S473), anti-EGFR (D38B1), anti–phospho-EGFR (Tyr^{1068}) (D7A5) (all from Cell Signaling Technology), anti–RAF-B (F-7), anti–α-tubulin (Santa Cruz Biotechnology), anti–glyceraldehyde-3-phosphate dehydrogenase (Abcam), and anti-HA (3F10) (Roche Diagnostics). Belvarafenib (HM95573), dabrafenib, encorafenib, GDC-0879, lifirafenib (BGB-283), LY3009120, MLN2480, naporafenib (LXH254), sorafenib, TAK-632, trametinib, vemurafenib, and XL888 were purchased from SelleckChem. All inhibitors were dissolved in dimethyl sulfoxide (DMSO).

Western blotting and BN-PAGE

Western blotting was carried out as previously described (*9*). Briefly, cells were lysed in normal lysis buffer [NLB; 50 mM tris/HCl (pH 7.5), 1% Triton X-100, 137 mM sodium chloride, 1% glycerine, 1 mM sodium orthovanadate, 0.5 mM EDTA, leupeptin (0.01 mg/ml), aprotinin (0.1 mg/ml), and 1 mM 4-(2-Aminoethyl)benzenesulfonyl fluoride hydrochloride (AEBSF)], separated on SDS gels containing 10% polyacrylamide and transferred to polyvinylidene difluoride membranes. Blotted proteins were visualized using

horseradish peroxidase–conjugated secondary antibodies (Thermo Fisher Scientific), SuperSignal West Femto Maximum Sensitivity Substrate (Thermo Fisher Scientific), and a Fusion Solo imaging system (Vilber). Signals were quantified using ImageJ.

For BN-PAGE, transiently transfected HEK293T cells were harvested 2 days after transfection. Before harvest, cell culture dishes were washed twice with ice-cold PBS. Ice-cold BN-PAGE lysis buffer [20 mM bis-tris, 20 mM NaCl, 2 mM EDTA, 10% glycerol, 0.1% Triton X-100, protease inhibitor cocktail (Roche, no. 11836145001), and PhoSTOP (Roche no. 04906837001) (pH 7)] was added directly to the plates, which were left on a rocking platform at 4°C for 30 min for cell lysis. Cells were scraped and lysates transferred into fresh reaction tubes and centrifuged at 4°C at 15,700*g* for 10 min, and supernatant was transferred into fresh reaction tubes for gel loading. BN-PAGE was performed according to instructions of the manufacturer [NativePAGE Novex 3 to 12% bis-tris protein gels, 1.0 mm, 10 well (Invitrogen, BN1001)] at 4°C. In brief, 50 μl of lysate were mixed with 150 μl of a glycerol-BN-PAGE lysis buffer solution (1:2). Wells were visualized for sample loading by flushing them two to three times with dark-blue cathode buffer (Invitrogen, BN2002), and the front part of the chamber was filled half with dark-blue cathode buffer. Twenty microliters of each sample was loaded into pockets. The front part of the chamber was completely filled with dark-blue cathode buffer, and afterward, the back part of the chamber was filled with transparent anode buffer (Invitrogen, BN2001). Proteins were separated at 100 V and 4°C for 60 min. Thereafter, the dark-blue cathode buffer was changed to light-blue cathode buffer (Invitrogen, BN2002), and the electrophoresis was continued at 200 V for additional 1 hour and 15 min, followed by Western blots. Signals were quantified using ImageJ.

Immunoprecipitations and MS

For immunoprecipitations, HEK293T cells transiently coexpressing HA- and Myc-BRAF proteins that were grown to subconfluency on a 10-cm dish were lysed in 1 ml of NLB 48 hours after transfection. Next, 0.5 μg of anti-HA antibody was added to 900 μl of cleared total cell lysates, followed by 1 hour of incubation on ice. Fifty microliters of Protein G-Sepharose slurry was added, followed by incubation at 4°C overnight, rotating. Beads were washed eight times with 1 ml of NLB. Following resuspension in 100 μl of NLB, addition of Laemmli buffer and boiling for 5 min, samples were analyzed via Western blotting.

For MS analysis of HSP90i-treated OV-90 cells ($BRAF^{WT/\Delta NVTAP}$), 40 15-cm dishes of subconfluent OV-90 cells were cultivated in the presence of XL888 (1 μM) or control (DMSO) for 24 hours before lysis in NLB (800 μl per dish). Cleared lysates were combined and incubated in the presence of an anti-BRAF antibody cocktail [150 μl of anti–RAF-B (F-7) and 100 μl of anti–B-RAF (D9T6S)] 1 hour on ice, followed by addition of 200 μl of Protein G-Sepharose slurry and incubation at 4°C overnight, rotating. Beads were washed five times and subjected to MS analysis.

For MS, samples were taken up in Laemmli sample buffer, reduced with 1 mM dithiothreitol for 10 min at 75°C, and alkylated using 5.5 mM iodoacetamide for 10 min at room temperature. The same amount of each sample was loaded on 4 to 12% gradients gels. The gel area corresponding to 80 to 100 kDa was excised and cut into small pieces, and proteins therein were in-gel digested with trypsin (Promega). Tryptic peptides were purified by STAGE tips before liquid chromatography tandem MS (LC-MS/MS) measurements. The LC-MS/MS measurements were performed on an Exploris 480 mass spectrometer coupled to an EasyLC 1200 nanoflow–high-performance liquid chromatography (HPLC). Peptides were separated on fused silica HPLC-column tip [inside diameter, 75 μm, New Objective, self-packed with reprosil-Pur 120 C18-AQ, 1.9 μm (Dr. Maisch) to a length of 20 cm] using a gradient of A (0.1% formic acid in water) and B (0.1% formic acid in 80% acetonitrile in water). A mass spectrometer was operated in the data-dependent mode; after each MS scan (mass range m/z = 370 to 1750; resolution, 120,000), a maximum of 20 MS/MS scans were performed using a normalized collision energy of 28%, a target value of 50%, and a resolution of 15,000. MS raw files were processed with MaxQuant software (version 2.0.1.0) using a Uniprot human database containing all BRAF variants and standard settings (*112*).

Transfection, infection, and focus formation assays

Transient transfection of Plat-E and HEK293T cells was carried out as previously described (*9*). For Western blot analysis, cells were lysed 48 hours after transfection. Viral supernatants of Plat-E cells were harvested and used for infection after 48 hours as well. Infection of MEFs and subsequent foci formation assays were carried out as described previously (*40*, *44*).

Colony formation assays

Cells were plated on six-well plates (1200 cells per well). Inhibitors were added the following day. Medium, supplemented with inhibitors, was changed every 2 to 3 days. Colonies of OV-90, BxPC3, and H2405 cells were stained with 0.1% crystal violet staining solution after 16, 18, or 21 days, respectively. Stained six-well plates were digitalized by scanning followed by quantification of colonized areas using ImageJ.

XTT assay

Cells were seeded onto 96-well plates (OV-90 and NCI-H2405 4000, BxPC3 2000 cells per well) and incubated with inhibitor or vehicle control (DMSO) for 96 hours. Inhibitor titrations were performed with a Tecan D300e device. Subsequently, the metabolic activity was measured using the Cell Proliferation Kit II (Roche Diagnostics) according to the manufacturer's protocol.

BRAF stability (tet washout) and HSP90 inhibition assays

To determine BRAF stability, pCLXEBR MEFs were grown in the presence of tet (20 μg/ml), which is less stable than its analog doxycycline, for 30 hours to induce expression of HA-BRAF proteins. Following tet washout to stop transcription of the BRAF expression cassette and a waiting time of 26 hours to allow for depletion of residual tet and tet-induced mRNA, cells were grown for the indicated times. BRAF levels were determined by Western blot and normalized to α-tubulin. Protein half-lives were calculated using one-phase decay function. To analyze the effect of HSP90 inhibition on the stability of BRAF proteins, pCLXEBR MEFs were grown in the presence of doxycycline (50 ng/ml). After 72 hours, the HSP90 inhibitor XL888 (1 μM) was added. Cells were subject to Western blot analysis after 0, 5, 8, and 24 hours after HSP90i.

Cellular thermal shift assay

HEK293T cells transiently expressing HA-BRAF proteins were detached by trypsin, suspended in DPBS (10×10^6 cells/ml), and incubated in the presence of 100 μM dabrafenib or vehicle control (DMSO) for 4 hours, rotating at room temperature. Cells were divided into 100 μl aliquots and heated in a PCR machine at increasing temperatures (42° to 54°C) for 3 min. Subsequently, lysis was performed in NLB for 10 min. Denatured and precipitated BRAF protein was removed by centrifugation at 16,000*g*, 4°C for 15 min. Levels of residual native BRAF protein were analyzed by Western blotting.

Statistical analysis

The number of individual experiments as well as the applied statistical tests were specified in the respective figure legend. Data are presented as means + SD, if not stated otherwise. Statistical analyses were performed using GraphPad Prism 9 (GraphPad Inc., CA).

Supplementary Materials

This PDF file includes:

Figs. S1 to S16
Table S1
References

REFERENCES AND NOTES

1. M. L. Turski, S. J. Vidwans, F. Janku, I. Garrido-Laguna, J. Munoz, R. Schwab, V. Subbiah, J. Rodon, R. Kurzrock, Genomically driven tumors and actionability across histologies: BRAF-mutant cancers as a paradigm. *Mol. Cancer Ther.* **15**, 533–547 (2016).
2. F. A. Cook, S. J. Cook, Inhibition of RAF dimers: It takes two to tango. *Biochem. Soc. Trans.* **49**, 237–251 (2021).
3. T. Brummer, C. McInnes, RAF kinase dimerization: Implications for drug discovery and clinical outcomes. *Oncogene* **39**, 4155–4169 (2020).
4. J. A. Martinez Fiesco, D. E. Durrant, D. K. Morrison, P. Zhang, Structural insights into the BRAF monomer-to-dimer transition mediated by RAS binding. *Nat. Commun.* **13**, 486 (2022).
5. Y. Kondo, J. Ognjenović, S. Banerjee, D. Karandur, A. Merk, K. Kulhanek, K. Wong, J. P. Roose, S. Subramaniam, J. Kuriyan, Cryo-EM structure of a dimeric B-Raf:14-3-3 complex reveals asymmetry in the active sites of B-Raf kinases. *Science* **366**, 109–115 (2019).
6. E. Park, S. Rawson, K. Li, B. W. Kim, S. B. Ficarro, G. G. D. Pino, H. Sharif, J. A. Marto, H. Jeon, M. J. Eck, Architecture of autoinhibited and active BRAF–MEK1–14-3-3 complexes. *Nature* **575**, 545–550 (2019).
7. R. Röck, J. E. Mayrhofer, O. Torres-Quesada, F. Enzler, A. Raffeiner, P. Raffeiner, A. Feichtner, R. G. Huber, S. Koide, S. S. Taylor, J. Troppmair, E. Stefan, BRAF inhibitors promote intermediate BRAF(V600E) conformations and binary interactions with activated RAS. *Sci. Adv.* **5**, eaav8463 (2019).
8. T. Rajakulendran, M. Sahmi, M. Lefrancois, F. Sicheri, M. Therrien, A dimerization-dependent mechanism drives RAF catalytic activation. *Nature* **461**, 542–545 (2009).
9. M. Röring, R. Herr, G. J. Fiala, K. Heilmann, S. Braun, A. E. Eisenhardt, S. Halbach, D. Capper, A. von Deimling, W. W. Schamel, D. N. Saunders, T. Brummer, Distinct requirement for an intact dimer interface in wild-type, V600E and kinase-dead B-Raf signalling. *EMBO J.* **31**, 2629–2647 (2012).
10. H. Lavoie, M. Therrien, Regulation of RAF protein kinases in ERK signalling. *Nat. Rev. Mol. Cell Biol.* **16**, 281–298 (2015).
11. A. K. Freeman, D. A. Ritt, D. K. Morrison, Effects of Raf dimerization and its inhibition on normal and disease-associated Raf signaling. *Mol. Cell* **49**, 751–758 (2013).
12. J. Hu, E. C. Stites, H. Yu, E. A. Germino, H. S. Meharena, P. J. S. Stork, A. P. Kornev, S. S. Taylor, A. S. Shaw, Allosteric activation of functionally asymmetric RAF kinase dimers. *Cell* **154**, 1036–1046 (2013).
13. Y. Kondo, J. W. Paul III, S. Subramaniam, J. Kuriyan, New insights into Raf regulation from structural analyses. *Curr. Opin. Struct. Biol.* **71**, 223–231 (2021).
14. H. R. Mott, D. Owen, SHOCing RAF into action. *Nat. Struct. Mol. Biol.* **29**, 958–960 (2022).
15. M. Zhang, R. Maloney, H. Jang, R. Nussinov, The mechanism of Raf activation through dimerization. *Chem. Sci.* **12**, 15609–15619 (2021).
16. B. H. Zhang, K. L. Guan, Activation of B-Raf kinase requires phosphorylation of the conserved residues Thr598 and Ser601. *EMBO J.* **19**, 5429–5439 (2000).
17. N. Thevakumaran, H. Lavoie, D. A. Critton, A. Tebben, A. Marinier, F. Sicheri, M. Therrien, Crystal structure of a BRAF kinase domain monomer explains basis for allosteric regulation. *Nat. Struct. Mol. Biol.* **22**, 37–43 (2015).
18. M. Köhler, M. Röring, B. Schorch, K. Heilmann, N. Stickel, G. J. Fiala, L. C. Schmitt, S. Braun, S. Ehrenfeld, F. M. Uhl, T. Kaltenbacher, F. Weinberg, S. Herzog, R. Zeiser, W. W. Schamel, H. Jumaa, T. Brummer, Activation loop phosphorylation regulates B-Raf in vivo and transformation by B-Raf mutants. *EMBO J.* **35**, 143–161 (2016).
19. B. Agianian, E. Gavathiotis, Current insights of BRAF inhibitors in cancer. *J. Med. Chem.* **61**, 5775–5793 (2018).
20. Z. Karoulia, E. Gavathiotis, P. I. Poulikakos, New perspectives for targeting RAF kinase in human cancer. *Nat. Rev. Cancer* **17**, 676–691 (2017).
21. Z. Yao, N. M. Torres, A. Tao, Y. Gao, L. Luo, Q. Li, E. de Stanchina, O. Abdel-Wahab, D. B. Solit, P. I. Poulikakos, N. Rosen, BRAF Mutants Evade ERK-dependent feedback by different mechanisms that determine their sensitivity to pharmacologic inhibition. *Cancer Cell* **28**, 370–383 (2015).
22. O. S. Rukhlenko, F. Khorsand, A. Krstic, J. Rozanc, L. G. Alexopoulos, N. Rauch, K. E. Erickson, W. S. Hlavacek, R. G. Posner, S. Gómez-Coca, E. Rosta, C. Fitzgibbon, D. Matallanas, J. Rauch, W. Kolch, B. N. Kholodenko, Dissecting RAF inhibitor resistance by structure-based modeling reveals ways to overcome oncogenic RAS signaling. *Cell Syst.* **7**, 161–179.e14 (2018).
23. B. Diedrich, K. T. G. Rigbolt, M. Röring, R. Herr, S. Kaeser-Pebernard, C. Gretzmeier, R. F. Murphy, T. Brummer, J. Dengjel, Discrete cytosolic macromolecular BRAF complexes exhibit distinct activities and composition. *EMBO J.* **36**, 646–663 (2017).
24. J. Yuan, W. H. Ng, P. Y. P. Lam, Y. Wang, H. Xia, J. Yap, S. P. Guan, A. S. G. Lee, M. Wang, M. Baccarini, J. Hu, The dimer-dependent catalytic activity of RAF family kinases is revealed through characterizing their oncogenic mutants. *Oncogene* **37**, 5719–5734 (2018).
25. C. Adamopoulos, T. A. Ahmed, M. R. Tucker, P. M. U. Ung, M. Xiao, Z. Karoulia, A. Amabile, X. Wu, S. A. Aaronson, C. Ang, V. W. Rebecca, B. D. Brown, A. Schlessinger, M. Herlyn, Q. Wang, D. E. Shaw, P. I. Poulikakos, Exploiting allosteric properties of RAF and MEK inhibitors to target therapy-resistant tumors driven by oncogenic BRAF signaling. *Cancer Discov.* **11**, 1716–1735 (2021).
26. M. Dankner, A. A. N. Rose, S. Rajkumar, P. M. Siegel, I. R. Watson, Classifying BRAF alterations in cancer: New rational therapeutic strategies for actionable mutations. *Oncogene* **37**, 3183–3199 (2018).
27. P. T. C. Wan, M. J. Garnett, S. M. Roe, S. Lee, D. Niculescu-Duvaz, V. M. Good, C. M. Jones, C. J. Marshall, C. J. Springer, D. Barford, R. Marais; Cancer Genome Project, Mechanism of activation of the RAF-ERK signaling pathway by oncogenic mutations of B-RAF. *Cell* **116**, 855–867 (2004).
28. S. J. Heidorn, C. Milagre, S. Whittaker, A. Nourry, I. Niculescu-Duvas, N. Dhomen, J. Hussain, J. S. Reis-Filho, C. J. Springer, C. Pritchard, R. Marais, Kinase-dead BRAF and oncogenic RAS cooperate to drive tumor progression through CRAF. *Cell* **140**, 209–221 (2010).
29. P. Nieto, C. Ambrogio, L. Esteban-Burgos, G. Gómez-López, M. T. Blasco, Z. Yao, R. Marais, N. Rosen, R. Chiarle, D. G. Pisano, M. Barbacid, D. Santamaría, A Braf kinase-inactive mutant induces lung adenocarcinoma. *Nature* **548**, 239–243 (2017).
30. M. Dankner, M. Lajoie, D. Moldoveanu, T. T. Nguyen, P. Savage, S. Rajkumar, X. Huang, M. Lvova, A. Protopopov, D. Vuzman, D. Hogg, M. Park, M. C. Guiot, K. Petrecca, C. Mihalcioiu, I. R. Watson, P. M. Siegel, A. A. N. Rose, Dual MAPK inhibition is an effective therapeutic strategy for a subset of class II BRAF mutant melanomas. *Clin. Cancer Res.* **24**, 6483–6494 (2018).
31. A. J. Aguirre, J. A. Nowak, N. D. Camarda, R. A. Moffitt, A. A. Ghazani, M. Hazar-Rethinam, S. Raghavan, J. Kim, L. K. Brais, D. Ragon, M. W. Welch, E. Reilly, D. McCabe, L. Marini, K. Anderka, K. Helvie, N. Oliver, A. Babic, A. da Silva, B. Nadres, E. E. van Seventer, H. A. Shahzade, J. P. St. Pierre, K. P. Burke, T. Clancy, J. M. Cleary, L. A. Doyle, K. Jajoo, N. J. McCleary, J. A. Meyerhardt, J. E. Murphy, K. Ng, A. K. Patel, K. Perez, M. H. Rosenthal, D. A. Rubinson, M. Ryou, G. I. Shapiro, E. Sicinska, S. G. Silverman, R. J. Nagy, R. B. Lanman, D. Knoerzer, D. J. Welsch, M. B. Yurgelun, C. S. Fuchs, L. A. Garraway, G. Getz, J. L. Hornick, B. E. Johnson, M. H. Kulke, R. J. Mayer, J. W. Miller, P. B. Shyn, D. A. Tuveson, N. Wagle, J. J. Yeh, W. C. Hahn, R. B. Corcoran, S. L. Carter, B. M. Wolpin, Real-time genomic characterization of advanced pancreatic cancer to enable precision medicine. *Cancer Discov.* **8**, 1096–1111 (2018).
32. P. A. Philip, I. Azar, J. Xiu, M. J. Hall, A. E. Hendifar, E. Lou, J. J. Hwang, J. Gong, R. Feldman, M. Ellis, P. Stafford, D. Spetzler, M. M. Khushman, D. Sohal, A. C. Lockhart, B. A. Weinberg, W. S. el-Deiry, J. Marshall, A. F. Shields, W. M. Korn, Molecular characterization of KRAS wild-type tumors in patients with pancreatic adenocarcinoma. *Clin. Cancer Res.* **28**, 2704–2714 (2022).

33. R. Ren, S. G. Krishna, W. Chen, W. L. Frankel, R. Shen, W. Zhao, M. R. Avenarius, J. Garee, S. Caruthers, D. Jones, Activation of the RAS pathway through uncommon BRAF mutations in mucinous pancreatic cysts without KRAS mutation. *Mod. Pathol.* **34**, 438–444 (2021).
34. A. Hendifar, E. M. Blais, B. Wolpin, V. Subbiah, E. Collisson, I. Singh, T. Cannon, K. Shaw, E. F. Petricoin III, S. Klempner, E. Lyons, A. Wang-Gillam, M. J. Pishvaian, E. M. O'Reilly, Retrospective case series analysis of *RAF* family alterations in pancreatic cancer: Real-world outcomes from targeted and standard therapies. *JCO Precis. Oncol.* **5**, PO.20.00494 (2021).
35. S. H. Chen, Y. Zhang, R. D. van Horn, T. Yin, S. Buchanan, V. Yadav, I. Mochalkin, S. S. Wong, Y. G. Yue, L. Huber, I. Conti, J. R. Henry, J. J. Starling, G. D. Plowman, S. B. Peng, Oncogenic braf deletions that function as homodimers and are sensitive to inhibition by RAF dimer inhibitor LY3009120. *Cancer Discov.* **6**, 300–315 (2016).
36. S. A. Foster, D. M. Whalen, A. Özen, M. J. Wongchenko, J. P. Yin, I. Yen, G. Schaefer, J. D. Mayfield, J. Chmielecki, P. J. Stephens, L. A. Albacker, Y. Yan, K. Song, G. Hatzivassiliou, C. Eigenbrot, C. Yu, A. S. Shaw, G. Manning, N. J. Skelton, S. G. Hymowitz, S. Malek, Activation mechanism of oncogenic deletion mutations in BRAF, EGFR, and HER2. *Cancer Cell* **29**, 477–493 (2016).
37. D. M. Freed, J. H. Park, R. Radhakrishnan, M. A. Lemmon, Deletion mutations keep kinase inhibitors in the loop. *Cancer Cell* **29**, 423–425 (2016).
38. P. Horak, C. Heining, S. Kreutzfeldt, B. Hutter, A. Mock, J. Hüllein, M. Fröhlich, S. Uhrig, A. Jahn, A. Rump, L. Gieldon, L. Möhrmann, D. Hanf, V. Teleanu, C. E. Heilig, D. B. Lipka, M. Allgäuer, L. Ruhnke, A. Laßmann, V. Endris, O. Neumann, R. Penzel, K. Beck, D. Richter, U. Winter, S. Wolf, K. Pfütze, C. Geörg, B. Meißburger, I. Buchhalter, M. Augustin, W. E. Aulitzky, P. Hohenberger, M. Kroiss, P. Schirmacher, R. F. Schlenk, U. Keilholz, F. Klauschen, G. Folprecht, S. Bauer, J. T. Siveke, C. H. Brandts, T. Kindler, M. Boerries, A. L. Illert, N. von Bubnoff, P. J. Jost, K. Spiekermann, M. Bitzer, K. Schulze-Osthoff, C. von Kalle, B. Klink, B. Brors, A. Stenzinger, E. Schröck, D. Hübschmann, W. Weichert, H. Glimm, S. Fröhling, Comprehensive genomic and transcriptomic analysis for guiding therapeutic decisions in patients with rare cancers. *Cancer Discov.* **11**, 2780–2795 (2021).
39. D. Pratt, S. Camelo-Piragua, K. McFadden, D. Leung, R. Mody, A. Chinnaiyan, C. Koschmann, S. Venneti, BRAF activating mutations involving the β3-αC loop in V600E-negative anaplastic pleomorphic xanthoastrocytoma. *Acta Neuropathol. Commun.* **6**, 24 (2018).
40. F. Weinberg, R. Griffin, M. Fröhlich, C. Heining, S. Braun, C. Spohr, M. Iconomou, V. Hollek, M. Röring, P. Horak, S. Kreutzfeldt, G. Warsow, B. Hutter, S. Uhrig, O. Neumann, D. Reuss, D. H. Heiland, C. von Kalle, W. Weichert, A. Stenzinger, B. Brors, H. Glimm, S. Fröhling, T. Brummer, Identification and characterization of a BRAF fusion oncoprotein with retained autoinhibitory domains. *Oncogene* **39**, 814–832 (2020).
41. J. Hu, L. G. Ahuja, H. S. Meharena, N. Kannan, A. P. Kornev, S. S. Taylor, A. S. Shaw, Kinase regulation by hydrophobic spine assembly in cancer. *Mol. Cell. Biol.* **35**, 264–276 (2015).
42. P. I. Poulikakos, Y. Persaud, M. Janakiraman, X. Kong, C. Ng, G. Moriceau, H. Shi, M. Atefi, B. Titz, M. T. Gabay, M. Salton, K. B. Dahlman, M. Tadi, J. A. Wargo, K. T. Flaherty, M. C. Kelley, T. Misteli, P. B. Chapman, J. A. Sosman, T. G. Graeber, A. Ribas, R. S. Lo, N. Rosen, D. B. Solit, RAF inhibitor resistance is mediated by dimerization of aberrantly spliced BRAF(V600E). *Nature* **480**, 387–390 (2011).
43. T. Ikenoue, Y. Hikiba, F. Kanai, Y. Tanaka, J. Imamura, T. Imamura, M. Ohta, H. Ijichi, K. Tateishi, T. Kawakami, J. Aragaki, M. Matsumura, T. Kawabe, M. Omata, Functional analysis of mutations within the kinase activation segment of *B-Raf* in human colorectal tumors. *Cancer Res.* **63**, 8132–8137 (2003).
44. M. Kordes, M. Röring, C. Heining, S. Braun, B. Hutter, D. Richter, C. Geörg, C. Scholl, S. Gröschel, W. Roth, A. Rosenwald, E. Geissinger, C. von Kalle, D. Jäger, B. Brors, W. Weichert, C. Grüllich, H. Glimm, T. Brummer, S. Fröhling, Cooperation of BRAF(F595L) and mutant HRAS in histiocytic sarcoma provides new insights into oncogenic BRAF signaling. *Leukemia* **30**, 937–946 (2016).
45. A. E. Eisenhardt, A. Sprenger, M. Röring, R. Herr, F. Weinberg, M. Köhler, S. Braun, J. Orth, B. Diedrich, U. Lanner, N. Tscherwinski, S. Schuster, N. Dumaz, E. Schmidt, R. Baumeister, A. Schlosser, J. Dengjel, T. Brummer, Phospho-proteomic analyses of B-Raf protein complexes reveal new regulatory principles. *Oncotarget* **7**, 26628–26652 (2016).
46. K. Miyamoto, M. Sawa, Development of highly sensitive biosensors of RAF dimerization in cells. *Sci. Rep.* **9**, 636 (2019).
47. S. da Rocha Dias, F. Friedlos, Y. Light, C. Springer, P. Workman, R. Marais, Activated B-RAF is an Hsp90 client protein that is targeted by the anticancer drug 17-allylamino-17-demethoxygeldanamycin. *Cancer Res.* **65**, 10686–10691 (2005).
48. O. M. Grbovic, A. D. Basso, A. Sawai, Q. Ye, P. Friedlander, D. Solit, N. Rosen, V600E B-Raf requires the Hsp90 chaperone for stability and is degraded in response to Hsp90 inhibitors. *Proc. Natl. Acad. Sci. U.S.A.* **103**, 57–62 (2006).
49. Z. Eroglu, Y. A. Chen, G. T. Gibney, J. S. Weber, R. R. Kudchadkar, N. I. Khushalani, J. Markowitz, A. S. Brohl, L. F. Tetteh, H. Ramadan, G. Arnone, J. Li, X. Zhao, R. Sharma, L. N. F. Darville, B. Fang, I. Smalley, J. L. Messina, J. M. Koomen, V. K. Sondak, K. S. M. Smalley, Combined BRAF and HSP90 inhibition in patients with unresectable BRAF (V600E)-mutant melanoma. *Clin. Cancer Res.* **24**, 5516–5524 (2018).
50. M. A. Hernandez, B. Patel, F. Hey, S. Giblett, H. Davis, C. Pritchard, Regulation of BRAF protein stability by a negative feedback loop involving the MEK-ERK pathway but not the FBXW7 tumour suppressor. *Cell. Signal.* **28**, 561–571 (2016).
51. J. M. Fernandes Neto, E. Nadal, E. Bosdriesz, S. N. Ooft, L. Farre, C. McLean, S. Klarenbeek, A. Jurgens, H. Hagen, L. Wang, E. Felip, A. Martinez-Marti, A. Vidal, E. Voest, L. F. A. Wessels, O. van Tellingen, A. Villanueva, R. Bernards, Multiple low dose therapy as an effective strategy to treat EGFR inhibitor-resistant NSCLC tumours. *Nat. Commun.* **11**, 3157 (2020).
52. R. J. Sullivan, A. Hollebecque, K. T. Flaherty, G. I. Shapiro, J. Rodon Ahnert, M. J. Millward, W. Zhang, L. Gao, A. Sykes, M. D. Willard, D. Yu, A. E. Schade, K. A. Crowe, D. L. Flynn, M. D. Kaufman, J. R. Henry, S. B. Peng, K. A. Benhadji, I. Conti, M. S. Gordon, R. V. Tiu, D. S. Hong, A phase I study of LY3009120, a pan-RAF inhibitor, in patients with advanced or metastatic cancer. *Mol. Cancer Ther.* **19**, 460–467 (2020).
53. I. Yen, F. Shanahan, J. Lee, Y. S. Hong, S. J. Shin, A. R. Moore, J. Sudhamsu, M. T. Chang, I. Bae, D. dela Cruz, T. Hunsaker, C. Klijn, N. P. D. Liau, E. Lin, S. E. Martin, Z. Modrusan, R. Piskol, E. Segal, A. Venkatanarayan, X. Ye, J. Yin, L. Zhang, J. S. Kim, H. S. Lim, K. P. Kim, Y. J. Kim, H. S. Han, S. J. Lee, S. T. Kim, M. Jung, Y. H. Hong, Y. S. Noh, M. Choi, O. Han, M. Nowicka, S. Srinivasan, Y. Yan, T. W. Kim, S. Malek, ARAF mutations confer resistance to the RAF inhibitor belvarafenib in melanoma. *Nature* **594**, 418–423 (2021).
54. K. A. Monaco, S. Delach, J. Yuan, Y. Mishina, P. Fordjour, E. Labrot, D. McKay, R. Guo, S. Higgins, H. Q. Wang, J. Liang, K. Bui, J. Green, P. Aspesi, J. Ambrose, F. Mapa, L. Griner, M. Jaskelioff, J. Fuller, K. Crawford, G. Pardee, S. Widger, P. S. Hammerman, J. A. Engelman, D. D. Stuart, V. G. Cooke, G. Caponigro, LXH254, a potent and selective ARAF-sparing inhibitor of BRAF and CRAF for the treatment of MAPK-driven tumors. *Clin. Cancer Res.* **27**, 2061–2073 (2021).
55. R. Herr, S. Halbach, M. Heizmann, H. Busch, M. Boerries, T. Brummer, BRAF inhibition upregulates a variety of receptor tyrosine kinases and their downstream effector Gab2 in colorectal cancer cell lines. *Oncogene* **37**, 1576–1593 (2018).
56. C. A. Pratilas, B. S. Taylor, Q. Ye, A. Viale, C. Sander, D. B. Solit, N. Rosen, (V600E)BRAF is associated with disabled feedback inhibition of RAF-MEK signaling and elevated transcriptional output of the pathway. *Proc. Natl. Acad. Sci. U.S.A.* **106**, 4519–4524 (2009).
57. J. Phuchareon, F. McCormick, D. W. Eisele, O. Tetsu, EGFR inhibition evokes innate drug resistance in lung cancer cells by preventing Akt activity and thus inactivating Ets-1 function. *Proc. Natl. Acad. Sci. U.S.A.* **112**, E3855–E3863 (2015).
58. N. Gutierrez-Prat, H. L. Zuberer, L. Mangano, Z. Karimaddini, L. Wolf, S. Tyanova, L. C. Wellinger, D. Marbach, V. Griesser, P. Pettazzoni, J. R. Bischoff, D. Rohle, C. Palladino, I. Vivanco, DUSP4 protects BRAF- and NRAS-mutant melanoma from oncogene overdose through modulation of MITF. *Life Sci. Alliance* **5**, e202101235 (2022).
59. D. M. Molina, R. Jafari, M. Ignatushchenko, T. Seki, E. A. Larsson, C. Dan, L. Sreekumar, Y. Cao, P. Nordlund, Monitoring drug target engagement in cells and tissues using the cellular thermal shift assay. *Science* **341**, 84–87 (2013).
60. M. Holderfield, M. M. Deuker, F. McCormick, M. McMahon, Targeting RAF kinases for cancer therapy: BRAF-mutated melanoma and beyond. *Nat. Rev. Cancer* **14**, 455–467 (2014).
61. P. I. Poulikakos, C. Zhang, G. Bollag, K. M. Shokat, N. Rosen, RAF inhibitors transactivate RAF dimers and ERK signalling in cells with wild-type BRAF. *Nature* **464**, 427–430 (2010).
62. D. N. Meijles, J. J. Cull, S. T. E. Cooper, T. Markou, M. A. Hardyman, S. J. Fuller, H. O. Alharbi, Z. H. R. Haines, V. Alcantara-Alonso, P. E. Glennon, M. N. Sheppard, P. H. Sugden, A. Clerk, The anti-cancer drug dabrafenib is not cardiotoxic and inhibits cardiac remodelling and fibrosis in a murine model of hypertension. *Clin. Sci. (Lond.)* **135**, 1631–1647 (2021).
63. T. R. Rheault, J. C. Stellwagen, G. M. Adjabeng, K. R. Hornberger, K. G. Petrov, A. G. Waterson, S. H. Dickerson, R. A. Mook Jr., S. G. Laquerre, A. J. King, O. W. Rossanese, M. R. Arnone, K. N. Smitheman, L. S. Kane-Carson, C. Han, G. S. Moorthy, K. G. Moss, D. E. Uehling, Discovery of dabrafenib: A selective inhibitor of raf kinases with antitumor activity against B-Raf-driven tumors. *ACS Med. Chem. Lett.* **4**, 358–362 (2013).
64. P. Koelblinger, O. Thuerigen, R. Dummer, Development of encorafenib for BRAF-mutated advanced melanoma. *Curr. Opin. Oncol.* **30**, 125–133 (2018).
65. X. M. Cotto-Rios, B. Agianian, N. Gitego, E. Zacharioudakis, O. Giricz, Y. Wu, Y. Zou, A. Verma, P. I. Poulikakos, E. Gavathiotis, Inhibitors of BRAF dimers using an allosteric site. *Nat. Commun.* **11**, 4370 (2020).
66. J. Yap, R. N. V. K. Deepak, Z. Tian, W. H. Ng, K. C. Goh, A. Foo, Z. H. Tee, M. P. Mohanam, Y. R. M. Sim, U. Degirmenci, P. Lam, Z. Chen, H. Fan, J. Hu, The stability of R-spine defines RAF inhibitor resistance: A comprehensive analysis of oncogenic BRAF mutants with in-frame insertion of αC-β4 loop. *Sci. Adv.* **7**, eabg0390 (2021).
67. D. M. Hyman, I. Puzanov, V. Subbiah, J. E. Faris, I. Chau, J. Y. Blay, J. Wolf, N. S. Raje, E. L. Diamond, A. Hollebecque, R. Gervais, M. E. Elez-Fernandez, A. Italiano, R. D. Hofheinz, M. Hidalgo, E. Chan, M. Schuler, S. F. Lasserre, M. Makrutzki, F. Sirzen, M. L. Veronese, J. Tabernero, J. Baselga, Vemurafenib in multiple nonmelanoma cancers with BRAF V600 mutations. *N. Engl. J. Med.* **373**, 726–736 (2015).

68. M. A. Gouda, V. Subbiah, Precision oncology for BRAF-mutant cancers with BRAF and MEK inhibitors: From melanoma to tissue-agnostic therapy. *ESMO Open* **8**, 100788 (2023).
69. M. H. Tan, N. J. Nowak, R. Loor, H. Ochi, A. A. Sandberg, C. Lopez, J. W. Pickren, R. Berjian, H. O. Douglass, T. M. Chu, Characterization of a new primary human pancreatic tumor line. *Cancer Invest.* **4**, 15–23 (1986).
70. L. G. Ahronian, E. M. Sennott, E. M. van Allen, N. Wagle, E. L. Kwak, J. E. Faris, J. T. Godfrey, K. Nishimura, K. D. Lynch, C. H. Mermel, E. L. Lockerman, A. Kalsy, J. M. Gurski Jr., S. Bahl, K. Anderka, L. M. Green, N. J. Lennon, T. G. Huynh, M. Mino-Kenudson, G. Getz, D. Dias-Santagata, A. J. Iafrate, J. A. Engelman, L. A. Garraway, R. B. Corcoran, Clinical acquired resistance to RAF inhibitor combinations in BRAF-mutant colorectal cancer through MAPK pathway alterations. *Cancer Discov.* **5**, 358–367 (2015).
71. K. S. M. Smalley, M. Xiao, J. Villanueva, T. K. Nguyen, K. T. Flaherty, R. Letrero, P. Van Belle, D. E. Elder, Y. Wang, K. L. Nathanson, M. Herlyn, CRAF inhibition induces apoptosis in melanoma cells with non-V600E BRAF mutations. *Oncogene* **28**, 85–94 (2009).
72. S. M. Wilhelm, C. Carter, L. Y. Tang, D. Wilkie, A. McNabola, H. Rong, C. Chen, X. Zhang, P. Vincent, M. McHugh, Y. Cao, J. Shujath, S. Gawlak, D. Eveleigh, B. Rowley, L. Liu, L. Adnane, M. Lynch, D. Auclair, I. Taylor, R. Gedrich, A. Voznesensky, B. Riedl, L. E. Post, G. Bollag, P. A. Trail, BAY 43-9006 exhibits broad spectrum oral antitumor activity and targets the RAF/MEK/ERK pathway and receptor tyrosine kinases involved in tumor progression and angiogenesis. *Cancer Res.* **64**, 7099–7109 (2004).
73. D. Strumberg, H. Richly, R. A. Hilger, N. Schleucher, S. Korfee, M. Tewes, M. Faghih, E. Brendel, D. Voliotis, C. G. Haase, B. Schwartz, A. Awada, R. Voigtmann, M. E. Scheulen, S. Seeber, Phase I clinical and pharmacokinetic study of the Novel Raf kinase and vascular endothelial growth factor receptor inhibitor BAY 43-9006 in patients with advanced refractory solid tumors. *J. Clin. Oncol.* **23**, 965–972 (2005).
74. A. Awada, A. Hendlisz, T. Gil, S. Bartholomeus, M. Mano, D. de Valeriola, D. Strumberg, E. Brendel, C. G. Haase, B. Schwartz, M. Piccart, Phase I safety and pharmacokinetics of BAY 43-9006 administered for 21 days on/7 days off in patients with advanced, refractory solid tumours. *Br. J. Cancer* **92**, 1855–1861 (2005).
75. R. J. Sullivan, J. R. Infante, F. Janku, D. J. L. Wong, J. A. Sosman, V. Keedy, M. R. Patel, G. I. Shapiro, J. W. Mier, A. W. Tolcher, A. Wang-Gillam, M. Sznol, K. Flaherty, E. Buchbinder, R. D. Carvajal, A. M. Varghese, M. E. Lacouture, A. Ribas, S. P. Patel, G. A. DeCrescenzo, C. M. Emery, A. L. Groover, S. Saha, M. Varterasian, D. J. Welsch, D. M. Hyman, B. T. Li, First-in-class ERK1/2 inhibitor ulixertinib (BVD-523) in patients with MAPK mutant advanced solid tumors: Results of a phase I dose-escalation and expansion study. *Cancer Discov.* **8**, 184–195 (2018).
76. R. Sigaud, L. Rösch, C. Gatzweiler, J. Benzel, L. von Soosten, H. Peterziel, F. Selt, S. Najafi, S. Ayhan, X. F. Gerloff, N. Hofmann, I. Büdenbender, L. Schmitt, K. I. Foerster, J. Burhenne, W. E. Haefeli, A. Korshunov, F. Sahm, C. M. van Tilburg, D. T. W. Jones, S. M. Pfister, D. Knoerzer, B. L. Kreider, M. Sauter, K. W. Pajtler, M. Zuckermann, I. Oehme, O. Witt, T. Milde, The first-in-class ERK inhibitor ulixertinib shows promising activity in mitogen-activated protein kinase (MAPK)-driven pediatric low-grade glioma models. *Neuro Oncol.* **25**, 566–579 (2023).
77. M. Ghasemi, T. Turnbull, S. Sebastian, I. Kempson, The MTT assay: Utility, limitations, pitfalls, and interpretation in bulk and single-cell analysis. *Int. J. Mol. Sci.* **22**, 12827 (2021).
78. A. Prahallad, C. Sun, S. Huang, F. di Nicolantonio, R. Salazar, D. Zecchin, R. L. Beijersbergen, A. Bardelli, R. Bernards, Unresponsiveness of colon cancer to BRAF(V600E) inhibition through feedback activation of EGFR. *Nature* **483**, 100–103 (2012).
79. R. B. Corcoran, H. Ebi, A. B. Turke, E. M. Coffee, M. Nishino, A. P. Cogdill, R. D. Brown, P. Della Pelle, D. Dias-Santagata, K. E. Hung, K. T. Flaherty, A. Piris, J. A. Wargo, J. Settleman, M. Mino-Kenudson, J. A. Engelman, EGFR-mediated re-activation of MAPK signaling contributes to insensitivity of BRAF mutant colorectal cancers to RAF inhibition with vemurafenib. *Cancer Discov.* **2**, 227–235 (2012).
80. K. Zmajkovicova, V. Jesenberger, F. Catalanotti, C. Baumgartner, G. Reyes, M. Baccarini, MEK1 is required for PTEN membrane recruitment, AKT regulation, and the maintenance of peripheral tolerance. *Mol. Cell* **50**, 43–55 (2013).
81. B. A. Hemmings, D. F. Restuccia, PI3K-PKB/Akt pathway. *Cold Spring Harb. Perspect. Biol.* **4**, a011189 (2012).
82. D. Brauswetter, B. Gurbi, A. Varga, E. Várkondi, R. Schwab, G. Bánhegyi, O. Fábián, G. Kéri, I. Vályi-Nagy, I. Peták, Molecular subtype specific efficacy of MEK inhibitors in pancreatic cancers. *PLOS ONE* **12**, e0185687 (2017).
83. R. Hoefflin, A. L. Geißler, R. Fritsch, R. Claus, J. Wehrle, P. Metzger, M. Reiser, L. Mehmed, L. Fauth, D. H. Heiland, T. Erbes, F. Stock, A. Csanadi, C. Miething, B. Weddeling, F. Meiss, D. von Bubnoff, C. Dierks, I. Ge, V. Brass, S. Heeg, H. Schäfer, M. Boeker, J. Rawluk, E. M. Botzenhart, G. Kayser, S. Hettmer, H. Busch, C. Peters, M. Werner, J. Duyster, T. Brummer, M. Boerries, S. Lassmann, N. von Bubnoff, Personalized clinical decision making through implementation of a molecular tumor board: A german single-center experience. *JCO Precis. Oncol.* **2**, 1–16 (2018).
84. R. Kim, E. Tan, E. Wang, A. Mahipal, D. T. Chen, B. Cao, F. Masawi, C. Machado, J. Yu, D. W. Kim, A phase I trial of trametinib in combination with sorafenib in patients with advanced hepatocellular cancer. *Oncologist* **25**, e1893–e1899 (2020).
85. F. de Braud, C. Dooms, R. S. Heist, C. Lebbe, M. Wermke, A. Gazzah, D. Schadendorf, P. Rutkowski, J. Wolf, P. A. Ascierto, I. Gil-Bazo, S. Kato, M. Wolodarski, M. McKean, E. Muñoz Couselo, M. Sebastian, A. Santoro, V. Cooke, L. Manganelli, K. Wan, A. Gaur, J. Kim, G. Caponigro, X. M. Couillebault, H. Evans, C. D. Campbell, S. Basu, M. Moschetta, A. Daud, Initial evidence for the efficacy of naporafenib in combination with trametinib in NRAS-mutant melanoma: Results from the expansion arm of a phase Ib, open-label study. *J. Clin. Oncol.* **41**, 2651–2660 (2023).
86. M. Phadke, G. T. Gibney, C. J. Rich, I. V. Fedorenko, Y. A. Chen, R. R. Kudchadkar, V. K. Sondak, J. Weber, J. L. Messina, K. S. M. Smalley, XL888 limits vemurafenib-induced proliferative skin events by suppressing paradoxical MAPK activation. *J. Invest. Dermatol.* **135**, 2542–2544 (2015).
87. S. A. K. Rasheed, L. V. Subramanyan, W. K. Lim, U. K. Udayappan, M. Wang, P. J. Casey, The emerging roles of Gα12/13 proteins on the hallmarks of cancer in solid tumors. *Oncogene* **41**, 147–158 (2022).
88. J. X. Zhang, M. Yun, Y. Xu, J. W. Chen, H. W. Weng, Z. S. Zheng, C. Chen, D. Xie, S. Ye, GNA13 as a prognostic factor and mediator of gastric cancer progression. *Oncotarget* **7**, 4414–4427 (2016).
89. K. O. Wrzeszczynski, S. Rahman, M. O. Frank, K. Arora, M. Shah, H. Geiger, V. Felice, D. Manaa, E. Dikoglu, D. Khaira, A. R. Chimpiri, V. V. Michelini, V. Jobanputra, R. B. Darnell, S. Powers, M. Choi, Identification of targetable BRAF ΔN486_P490 variant by whole-genome sequencing leading to dabrafenib-induced remission of a BRAF-mutant pancreatic adenocarcinoma. *Cold Spring Harb. Mol. Case Stud.* **5**, a004424 (2019).
90. A. D. Singhi, B. George, J. R. Greenbowe, J. Chung, J. Suh, A. Maitra, S. J. Klempner, A. Hendifar, J. M. Milind, T. Golan, R. E. Brand, A. H. Zureikat, S. Roy, A. B. Schrock, V. A. Miller, J. S. Ross, S. M. Ali, N. Bahary, Real-time targeted genome profile analysis of pancreatic ductal adenocarcinomas identifies genetic alterations that might be targeted with existing drugs or used as biomarkers. *Gastroenterology* **156**, 2242–2253.e4 (2019).
91. F. Bray, J. Ferlay, I. Soerjomataram, R. L. Siegel, L. A. Torre, A. Jemal, Global cancer statistics 2018: GLOBOCAN estimates of incidence and mortality worldwide for 36 cancers in 185 countries. *CA Cancer J. Clin.* **68**, 394–424 (2018).
92. R. Thomas, C. A. Wiley, E. L. Droste, J. Robertson, B. A. Inman, M. Breen, Whole exome sequencing analysis of canine urothelial carcinomas without BRAF V595E mutation: Short in-frame deletions in BRAF and MAP2K1 suggest alternative mechanisms for MAPK pathway disruption. *PLOS Genet.* **19**, e1010575 (2023).
93. A. S. Shaw, A. P. Kornev, J. Hu, L. G. Ahuja, S. S. Taylor, Kinases and pseudokinases: Lessons from RAF. *Mol. Cell. Biol.* **34**, 1538–1546 (2014).
94. E. L. Diamond, B. H. Durham, G. A. Ulaner, E. Drill, J. Buthorn, M. Ki, L. Bitner, H. Cho, R. J. Young, J. H. Francis, R. Rampal, M. Lacouture, L. A. Brody, N. Ozkaya, A. Dogan, N. Rosen, A. Iasonos, O. Abdel-Wahab, D. M. Hyman, Efficacy of MEK inhibition in patients with histiocytic neoplasms. *Nature* **567**, 521–524 (2019).
95. Z. Eroglu, A. Ribas, Combination therapy with BRAF and MEK inhibitors for melanoma: Latest evidence and place in therapy. *Ther. Adv. Med. Oncol.* **8**, 48–56 (2016).
96. I. Ozkan-Dagliyan, J. N. Diehl, S. D. George, A. Schaefer, B. Papke, K. Klotz-Noack, A. M. Waters, C. M. Goodwin, P. Gautam, M. Pierobon, S. Peng, T. S. K. Gilbert, K. H. Lin, O. Dagliyan, K. Wennerberg, E. F. Petricoin III, N. L. Tran, S. V. Bhagwat, R. V. Tiu, S. B. Peng, L. E. Herring, L. M. Graves, C. Sers, K. C. Wood, A. D. Cox, C. J. Der, Low-dose vertical inhibition of the RAF-MEK-ERK cascade causes apoptotic death of KRAS mutant cancers. *Cell Rep.* **31**, 107764 (2020).
97. J. E. Shin, H. J. An, H. S. Park, H. Kim, B. Y. Shim, Efficacy of dabrafenib/trametinib in pancreatic ductal adenocarcinoma with BRAF NVTAP deletion: A case report. *Front. Oncol.* **12**, 976450 (2022).
98. R. Renier, P. De Haes, F. Bosisio, I. V. Bempt, A. J. F. Woei, Vulvar Langerhans cell histiocytosis: Clinicopathologic characteristics, mutational profile, and treatment of 4 patients in a single-center cohort. *JAAD Case Rep.* **36**, 78–81 (2023).
99. S. Zhang, Z. Yang, Y. Cheng, X. Guo, C. Liu, S. Wang, L. Zhang, BRAF L485-P490 deletion mutant metastatic melanoma sensitive to BRAF and MEK inhibition: A case report and literature review. *Front. Pharmacol.* **13**, 1019217 (2022).
100. J. Oberoi, X. A. Guiu, E. A. Outwin, P. Schellenberger, T. I. Roumeliotis, J. S. Choudhary, L. H. Pearl, HSP90-CDC37-PP5 forms a structural platform for kinase dephosphorylation. *Nat. Commun.* **13**, 7343 (2022).
101. S. García-Alonso, P. Mesa, L. de la Puente Ovejero, G. Aizpurua, C. G. Lechuga, E. Zarzuela, C. M. Santiveri, M. Sanclemente, J. Muñoz, M. Musteanu, R. Campos-Olivas, J. Martínez-Torrecuadrada, M. Barbacid, G. Montoya, Structure of the RAF1-HSP90-CDC37 complex reveals the basis of RAF1 regulation. *Mol. Cell* **82**, 3438–3452.e8 (2022).
102. D. Keramisanou, M. V. Vasantha Kumar, N. Boose, R. R. Abzalimov, I. Gelis, Assembly mechanism of early Hsp90-Cdc37-kinase complexes. *Sci. Adv.* **8**, eabm9294 (2022).

103. D. M. Bjorklund, R. M. L. Morgan, J. Oberoi, K. L. I. M. Day, P. A. Galliou, C. Prodromou, Recognition of BRAF by CDC37 and reevaluation of the activation mechanism for the class 2 BRAF-L597R mutant. *Biomolecules* **12**, 905 (2022).
104. P. Horak, B. Klink, C. Heining, S. Gröschel, B. Hutter, M. Fröhlich, S. Uhrig, D. Hübschmann, M. Schlesner, R. Eils, D. Richter, K. Pfütze, C. Geörg, B. Meißburger, S. Wolf, A. Schulz, R. Penzel, E. Herpel, M. Kirchner, A. Lier, V. Endris, S. Singer, P. Schirmacher, W. Weichert, A. Stenzinger, R. F. Schlenk, E. Schröck, B. Brors, C. von Kalle, H. Glimm, S. Fröhling, Precision oncology based on omics data: The NCT Heidelberg experience. *Int. J. Cancer* **141**, 877–886 (2017).
105. G. M. O'Kane, B. T. Grünwald, G.-H. Jang, M. Masoomian, S. Picardo, R. C. Grant, R. E. Denroche, A. Zhang, Y. Wang, B. Lam, P. M. Krzyzanowski, I. M. Lungu, J. M. S. Bartlett, M. Peralta, F. Vyas, R. Khokha, J. Biagi, D. Chadwick, S. Ramotar, S. Hutchinson, A. Dodd, J. M. Wilson, F. Notta, G. Zogopoulos, S. Gallinger, J. J. Knox, S. E. Fischer, GATA6 expression distinguishes classical and basal-like subtypes in advanced pancreatic cancer. *Clin. Cancer Res.* **26**, 4901–4910 (2020).
106. K. L. Aung, S. E. Fischer, R. E. Denroche, G. H. Jang, A. Dodd, S. Creighton, B. Southwood, S. B. Liang, D. Chadwick, A. Zhang, G. M. O'Kane, H. Albaba, S. Moura, R. C. Grant, J. K. Miller, F. Mbabaali, D. Pasternack, I. M. Lungu, J. M. S. Bartlett, S. Ghai, M. Lemire, S. Holter, A. A. Connor, R. A. Moffitt, J. J. Yeh, L. Timms, P. M. Krzyzanowski, N. Dhani, D. Hedley, F. Notta, J. M. Wilson, M. J. Moore, S. Gallinger, J. J. Knox, Genomics-driven precision medicine for advanced pancreatic cancer: Early results from the COMPASS trial. *Clin. Cancer Res.* **24**, 1344–1354 (2018).
107. N. A. Pham, N. Radulovich, E. Ibrahimov, S. N. Martins-Filho, Q. Li, M. Pintilie, J. Weiss, V. Raghavan, M. Cabanero, R. E. Denroche, J. M. Wilson, C. Metran-Nascente, A. Borgida, S. Hutchinson, A. Dodd, M. Begora, D. Chadwick, S. Serra, J. J. Knox, S. Gallinger, D. W. Hedley, L. Muthuswamy, M. S. Tsao, Patient-derived tumor xenograft and organoid models established from resected pancreatic, duodenal and biliary cancers. *Sci. Rep.* **11**, 10619 (2021).
108. L. A. Baker, H. Tiriac, D. A. Tuveson, Generation and culture of human pancreatic ductal adenocarcinoma organoids from resected tumor specimens. *Methods Mol. Biol.* **1882**, 97–115 (2019).
109. S. F. Boj, C. I. Hwang, L. A. Baker, D. D. Engle, D. A. Tuveson, H. Clevers, Model organoids provide new research opportunities for ductal pancreatic cancer. *Mol. Cell. Oncol.* **3**, e1014757 (2016).
110. G. Galabova-Kovacs, D. Matzen, D. Piazzolla, K. Meissl, T. Plyushch, A. P. Chen, A. Silva, M. Baccarini, Essential role of B-Raf in ERK activation during extraembryonic development. *Proc. Natl. Acad. Sci. U.S.A.* **103**, 1325–1330 (2006).
111. J. Albers, C. Danzer, M. Rechsteiner, H. Lehmann, L. P. Brandt, T. Hejhal, A. Catalano, P. Busenhart, A. F. Gonçalves, S. Brandt, P. K. Bode, B. Bode-Lesniewska, P. J. Wild, I. J. Frew, A versatile modular vector system for rapid combinatorial mammalian genetics. *J. Clin. Invest.* **125**, 1603–1619 (2015).
112. J. Cox, M. Mann, MaxQuant enables high peptide identification rates, individualized p.p.b.-range mass accuracies and proteome-wide protein quantification. *Nat. Biotechnol.* **26**, 1367–1372 (2008).
113. N. P. D. Liau, A. Venkatanarayan, J. G. Quinn, W. Phung, S. Malek, S. G. Hymowitz, J. Sudhamsu, Dimerization induced by C-terminal 14-3-3 binding is sufficient for BRAF kinase activation. *Biochemistry* **59**, 3982–3992 (2020).
114. B. Zhang, Y. Chen, P. Dai, H. Yu, J. Ma, C. Chen, Y. Zhang, Y. Guan, R. Chen, T. Liu, J. Wang, L. Yang, X. Yi, X. Xia, H. Ma, Oncogenic mutations within the beta3-alphaC loop of EGFR/ERBB2/BRAF/MAP2K1 predict response to therapies. *Mol. Genet. Genomic Med.* **8**, e1395 (2020).
115. B. S. White, I. Lanc, J. O'Neal, H. Gupta, R. S. Fulton, H. Schmidt, C. Fronick, E. A. Belter Jr., M. Fiala, J. King, G. J. Ahmann, M. DeRome, E. R. Mardis, R. Vij, J. F. DiPersio, J. Levy, D. Auclair, M. H. Tomasson, A multiple myeloma-specific capture sequencing platform discovers novel translocations and frequent, risk-associated point mutations in IGLL5. *Blood Cancer J.* **8**, 35 (2018).
116. M. Mirdita, K. Schütze, Y. Moriwaki, L. Heo, S. Ovchinnikov, M. Steinegger, ColabFold: Making protein folding accessible to all. *Nat. Methods* **19**, 679–682 (2022).

Acknowledgments

Funding: This work was supported by the German Research Foundation (DFG) through a Heisenberg professorship (T.B.; BR 3662/5–1) and the joint D-A-CH funding scheme between the DFG (T.B.; BR3662/4–1) and the Swiss National Science Foundation (J.D.; SNSF, 310030E_184433); SFB 1479—project ID: 441891347 [P14 (T.B.) and S1 (M.Bo.)], SFB 850 to R.F. and M.Bo.; the German Cancer Consortium DKTK through SORATRAM (T.B. and S.F.) and NCT/DKTK MASTER supported by the NCT Molecular Precision Oncology Program and the DKTK Joint Funding Program (H.G. and S.F.), the Ministry for Science, Research and Arts of the State of Baden-Wuerttemberg BW-VAPO (T.B., S.F., M.Bo., and M.Bi.), and the Canton and the University of Fribourg (J.D.). J.D. is member of the SKINTEGRITY.CH collaborative research project. The COMPASS study was conducted with the support of the Ontario Institute for Cancer Research (PanCuRx Translational Research Initiative) through funding provided by the Government of Ontario, the Wallace McCain Centre for Pancreatic Cancer supported by the Princess Margaret Cancer Foundation, the Terry Fox Research Institute, the Canadian Cancer Society Research Institute, and the Pancreatic Cancer Canada Foundation. The study was also supported by a charitable donation from the Canadian Friends of the Hebrew University (A. U. Soyka). **Author contributions:** Most experiments were performed by M.L. D.C., R.F.U.K., C.R., M.S., N.R., L.T., and I.X. also conducted experiments. R.F.U.K., J.K., N.R., L.T., I.X., U.A.W., M.Bo., C.R.B., S.G., R.F., and G.O. were involved in the establishment and initial characterization of PDOs. C.E.H., J.K., P.H., A.F., M.Bi., U.A.W., M.Bo., C.R.B., C.H., H.G., M.F., D.H., S.G., S.F., R.F., and G.O. provided clinical data and expertise as well as bioinformatic analyses on tumor genomes. D.C., R.F.U.K., and N.R. designed and analyzed experiments. M.L., J.D., and T.B. established the concept of the study and designed and analyzed experiments. Visualization was conducted by M.L. Project was supervised by H.G. and S.F. (clinical data) and J.D. and T.B. (wet laboratory). The paper was written by M.L. and T.B. with input from all authors. **Competing interests:** C.H. received honoraria from Roche and Novartis as well as research funding from Boehringer Ingelheim and has been consulting for Boehringer Ingelheim. G.O. received honoraria from AstraZeneca, Roche, Servier, MSD, Incyte, and Eisai and received funding from Roche. The authors declare that they have no other competing interests. **Data and materials availability:** All data needed to evaluate the conclusions in the paper are present in the paper and/or the Supplementary Materials. The plasmids used in this study can be provided by T.B. Requests for the plasmids should be submitted to tilman.brummer@mol-med.uni-freiburg.de.

Submitted 8 September 2022
Accepted 2 August 2023
Published 1 September 2023
10.1126/sciadv.ade7486